

# Experimental determination of Ramsey numbers

Zhengbing Bian,<sup>1</sup> Fabian Chudak,<sup>1</sup> William G. Macready,<sup>1</sup> Lane Clark,<sup>2</sup> and Frank Gaitan<sup>3</sup>

<sup>1</sup>*D-Wave Systems, Inc., 100-4401 Still Creek Drive, Burnaby, British Columbia V5C 6G9, Canada*

<sup>2</sup>*Department of Mathematics, Southern Illinois University, Carbondale, IL 62901-4401*

<sup>3</sup>*Laboratory for Physical Sciences, 8050 Greenmead Dr, College Park, MD 20740*

(Dated: November 1, 2018)

Ramsey theory is a highly active research area in mathematics that studies the emergence of order in large disordered structures. Ramsey numbers mark the threshold at which order first appears and are extremely difficult to calculate due to their explosive rate of growth. Recently, an algorithm that can be implemented using adiabatic quantum evolution has been proposed that calculates the two-color Ramsey numbers  $R(m, n)$ . Here we present results of an experimental implementation of this algorithm and show that it correctly determines the Ramsey numbers  $R(3, 3)$  and  $R(m, 2)$  for  $4 \leq m \leq 8$ . The  $R(8, 2)$  computation used 84 qubits of which 28 were computational qubits. This computation is the largest experimental implementation of a scientifically meaningful adiabatic evolution algorithm that has been done to date.

PACS numbers: 03.67.Ac, 02.10.Ox, 89.75.Hc

In recent years first steps have been taken towards experimentally realizing the computational advantages promised by well-known quantum algorithms. As with any nascent effort, these initial steps have been limited. To date the largest experimental implementations of scientifically meaningful quantum algorithms have used just a handful of qubits. For circuit-based algorithms,<sup>1</sup> *seven* spin-qubits were used to factor 15; while for adiabatic algorithms,<sup>2</sup> *four* spin-qubits were used to factor 143. In *both* cases compiled versions of the algorithms were needed to allow factoring with such small numbers of qubits. Although factoring was the focus of both experiments, other scientifically significant applications exist.

In Ref. 3 an algorithm for determining the two-color Ramsey numbers was proposed which could be implemented using adiabatic quantum evolution. Ramsey numbers are part of an active research area in mathematics known as Ramsey theory<sup>4</sup> whose central theme is the emergence of order in large disordered structures. The disordered structures can be represented by an  $N$ -vertex graph  $G$ , and the ordered substructures by specific graphs  $H_1$  and  $H_2$  that are to appear as subgraphs of  $G$ . For two-color Ramsey numbers the subgraphs  $H_1$  and  $H_2$  are  $m$ -cliques and  $n$ -independent sets, respectively. An  $m$ -clique is a set of  $m$  vertices that has an edge connecting any two of the  $m$  vertices, and an  $n$ -independent set is a set of  $n$  vertices in which no two of the  $n$  vertices is joined by an edge. Using Ramsey theory<sup>4,5</sup>, one can prove that a threshold value  $R(m, n)$  exists so that for  $N \geq R(m, n)$ , *every* graph with  $N$  vertices will contain either an  $m$ -clique or an  $n$ -independent set. The threshold value  $R(m, n)$  is an example of a two-color Ramsey number. Other types of Ramsey numbers exist, though we focus on two-color Ramsey numbers here. Ramsey numbers  $R(m, n)$  grow extremely quickly and are notoriously difficult to calculate. In fact, for  $m, n \geq 3$ , only nine are presently known<sup>5</sup>.

In the Ramsey number algorithm<sup>3</sup> (RNA) the calculation of  $R(m, n)$  is formulated as an optimization problem

which can be solved using adiabatic quantum evolution.<sup>6</sup> Here we present evidence of an *experimental* implementation of the RNA using adiabatic quantum evolution and show that it correctly determines the Ramsey numbers  $R(3, 3)$  and  $R(m, 2)$  for  $4 \leq m \leq 8$ . The experimental computation of  $R(8, 2)$  used a total of 84 qubits of which 28 were computational qubits, and applied an effective interaction coupling 28 qubits. To the best of our knowledge, this is the largest experimental implementation of a scientifically meaningful adiabatic evolution algorithm.

We begin this Letter with a brief description of the RNA. We then discuss the details of experimentally implementing the RNA using adiabatic quantum evolution on a chip of 106 superconducting flux qubits, and follow with a presentation of our experimental results. Finally, we close with a discussion of what has been found.

**1. Ramsey number algorithm:** We briefly describe the construction of the RNA; see Ref. 3 and the Supplementary Information (SI) for a detailed presentation.

As computation of  $R(m, n)$  is intimately connected with the presence/absence of edges, we associate a bit-variable  $a_{v,v'}$  with each pair of vertices  $(v, v')$  in an  $N$ -vertex graph  $G$ , and set  $a_{v,v'} = 1$  (0) when  $v$  and  $v'$  are (are not) joined by an edge in  $G$ . There are thus  $L_N = \binom{N}{2} \equiv N(N-1)/2$  bit-variables which we collect into the bit-vector (bit-string)  $\mathbf{a} = (a_{2,1}, \dots, a_{N,1}, a_{3,2}, \dots, a_{N,2}, \dots, a_{N,N-1})$  of length  $L_N$ . Thus an  $N$ -vertex graph  $G$  determines a unique bit-string  $\mathbf{a}$ , and vice versa. Ref. 3 (and the SI) showed how to count the number of  $m$ -cliques  $C_m^N(\mathbf{a})$  and  $n$ -independent sets  $I_n^N(\mathbf{a})$  in an  $N$ -vertex graph  $G$  using its associated bit-string  $\mathbf{a}$ . We can thus calculate the total number of  $m$ -cliques and  $n$ -independent sets contained in  $G$ :  $h_{m,n}^N(\mathbf{a}) = C_m^N(\mathbf{a}) + I_n^N(\mathbf{a})$ . Now consider the following combinatorial optimization problem (COP): For given integers  $(N, m, n)$  and cost function  $h_{m,n}^N(\mathbf{a})$  defined as above, find an  $N$ -vertex graph  $G_{\mathbf{a}_*}$  that yields the global minimum of  $h_{m,n}^N(\mathbf{a})$ . Notice that if  $N < R(m, n)$ , the global minimum is  $h_{m,n}^N(\mathbf{a}_*) = 0$  since Ramsey theory

guarantees that a graph exists that has no  $m$ -clique or  $n$ -independent set. Furthermore, if  $N \geq R(m, n)$ , Ramsey theory guarantees that  $h_{m,n}^N(\mathbf{a}_*) > 0$ .

Adiabatic quantum optimization (AQO)<sup>6</sup> is a  $T = 0$  ground-state method that exploits the adiabatic evolution of a quantum system to solve COPs, while quantum annealing (QA)<sup>7</sup> is a finite temperature method which can also be used to solve COPs even in the presence of decoherence. Ref. 3 described a quantum implementation of the RNA using AQO, while in this Letter we present evidence for a QA implementation of the RNA. (Note that a classical implementation of the RNA is also possible using a classical optimization algorithm run on a classical computer to solve the Ramsey number COP.) Both AQO and QA use the COP cost function to define a problem Hamiltonian  $H_P$  whose ground-state eigenspace contains all COP solutions. These algorithms evolve the state of a qubit register from the ground-state of an initial Hamiltonian  $H_i$  to a ground-state of  $H_P$  with high probability in the adiabatic limit. The algorithm dynamics is driven by a time-dependent Hamiltonian  $H(t) = A(t/t_f)H_i + B(t/t_f)H_P$ , where  $t_f$  is the algorithm run-time, adiabatic dynamics corresponds to  $t_f \rightarrow \infty$ , and  $A(t/t_f)$  ( $B(t/t_f)$ ) is a positive monotonically decreasing (increasing) function with  $A(1) = 0$  ( $B(0) = 0$ ).

In the quantum implementation of the RNA each bit-variable  $a_{v,v'}$  is promoted to a qubit, thus associating a qubit with each vertex pair  $(v, v')$ . The bit-strings  $\mathbf{a}$  now label the computational basis (CB) states  $|\mathbf{a}\rangle$ , and the problem Hamiltonian  $H_P$  is defined to be diagonal in the CB with eigenvalue  $h_{m,n}^N(\mathbf{a})$ . By construction, the ground-state energy of  $H_P$  vanishes if and only if there is a graph with no  $m$ -cliques or  $n$ -independent sets. The initial Hamiltonian  $H_i$  is the standard one for AQO<sup>6</sup> and appears in the SI. Its unique ground-state is the uniform superposition of all CB states.

Implementation of the RNA using QA computes  $R(m, n)$  as follows. First, choose  $N$  such that  $N < R(m, n)$ , then run QA on the  $L_N$  qubits and measure the qubits in the CB at the end of the anneal. This yields a bit-string  $\mathbf{a}_*$  which determines the final energy  $E = h_{m,n}^N(\mathbf{a}_*)$ . In the adiabatic limit the result will be  $E = 0$  since  $N < R(m, n)$ . Now increment  $N \rightarrow N + 1$ , re-run QA on the  $L_{N+1}$  qubits, and measure the final energy. Repeatedly increment  $N$  until  $E > 0$  first occurs, at which point the current value of  $N$  will be equal to  $R(m, n)$ . In any real application of the above algorithm the evolution will only be approximately adiabatic, and the probability that the measured energy will be the ground-state energy will thus be  $1 - \epsilon$ . By running the algorithm  $k \sim \mathcal{O}(\ln[1 - \delta]/\ln \epsilon)$  times, the probability  $\delta$  that at least one of the measurement outcomes yields the ground-state energy can be made arbitrarily close to 1.

**2. Experimental implementation:** Our hardware is designed to implement QA using RF-SQUID flux qubits. Each qubit is a superconducting loop interrupted by Josephson junctions, and the states  $|0\rangle$  and  $|1\rangle$  corre-

spond to the two directions of circulating current about the loop.<sup>8</sup> The chip hardware uses Josephson-junction-based devices to produce pairwise qubit-coupling.<sup>9</sup> By rescaling the chip Hamiltonian by the inter-qubit coupling energy  $J_{AFM}(t) = M_{AFM}|I_q^p(t)|^2$ , the low energy dynamics of the chip can be represented by a quantum Ising model in a transverse field with Hamiltonian:<sup>10</sup>

$$H = -A \left( \frac{t}{t_f} \right) \sum_i \sigma_i^x + B \left( \frac{t}{t_f} \right) \left\{ \sum_i h_i \sigma_i^z + \sum_{(i,j) \in E} J_{ij} \sigma_i^z \sigma_j^z \right\}.$$

Here  $M_{AFM}$  is the maximum value of the inter-qubit effective mutual inductance that the hardware can produce, and  $I_q^p(t)$  is the supercurrent circulating about the RF-SQUID loop. Although the scale factor  $J_{AFM}(t)$  is time-dependent, its order-of-magnitude can be estimated. For the D-Wave One device,  $M_{AFM} = 1.8pH$ , and  $|I_q^p(t)| \sim 0.6\mu A$  at the quantum critical point, so that  $J_{AFM} \sim 1GHz$  or  $50mK$ . With this rescaling, the local biases  $\{h_i\}$  and coupling strengths  $\{J_{ij}\}$  may be programmed to values in the ranges  $[-2, 2]$  and  $[-1, 1]$  respectively, and the experimentally measured functional forms of the interpolation functions  $A(t/t_f)$  and  $B(t/t_f)$  appear in the SI, along with the layout of qubits and couplers on the chip. For further details of the chip hardware, see Ref. 11.

The cost function  $h_{m,n}^N(\mathbf{a})$  is not yet ready for experimental implementation for two reasons: (a) there are  $k$ -qubit interactions with  $k > 2$ ; and (b) the qubit couplings do not correspond to the qubit couplings on the chip. These obstacles are removed as follows.

(a) *Reduction to pairwise coupling:* The SI shows that  $C_m^N(\mathbf{a})$  involves interactions coupling  $\binom{m}{2}$  qubits, while  $I_n^N(\mathbf{a})$  couples  $\binom{n}{2}$  qubits. These interactions must be reduced to pairwise coupling if  $h_{m,n}^N(\mathbf{a})$  is to be realized experimentally. We illustrate how such a reduction can be achieved by reducing the 3-bit coupling term  $a_1 a_2 a_3$  to pairwise coupling using an ancillary bit-variable  $b$  and penalty function  $P(a_1, a_2; b) = a_1 a_2 - 2(a_1 + a_2)b + 3b$ . Notice that  $P(a_1, a_2; b) = 0$  ( $> 0$ ) when the input values for  $a_1$ ,  $a_2$ , and  $b$  satisfy  $b = a_1 a_2$  ( $b \neq a_1 a_2$ ). Now consider the quadratic cost function  $h(b) = b a_3 + \mu P(a_1, a_2; b)$  for given values of  $\mu$  and  $a_i$ . For  $\mu$  sufficiently large,  $h(b)$  is minimized when  $b$  satisfies the equality constraint  $b = a_1 a_2$  which causes the penalty function to vanish. The optimum cost is then  $h(b = a_1 a_2) = a_1 a_2 a_3$  which reproduces the 3-bit coupling term using a quadratic cost function. This example is generalized in the SI to produce the quadratic cost function used to calculate  $R(m, 2)$ .

(b) *Matching spin to qubit connectivity:* A cost function with only pairwise qubit coupling may still not be experimentally realizable as the qubit couplings needed may not match the qubit couplings available on chip. The primal graph (PG) of a quadratic cost function is the graph whose vertices are the qubit variables, and whose edges indicate pairwise-coupled qubits. An arbitrary PG can be embedded into a sufficiently large qubit graph having the qubit layout and connectivity present on the

chip. An embedding maps a PG vertex to one or more vertices in the qubit graph, where the image vertices form a connected subgraph of the qubit graph. We link this connected set of qubits together with strong ferromagnetic couplings of strength  $\lambda$  so that in the lowest energy state these qubits have identical Bloch vectors. An example of this ferromagnetic coupling procedure is given in the SI.

**3. Embedding Ramsey problems:** We examined all Ramsey number COPs that could be solved using the 106 qubits available on the chip. Specifically,  $R(m, 2)$  with  $4 \leq m \leq 8$ , and  $R(3, 3)$ . Here we describe the embedding of these problems on to the chip.

(a)  $R(m, 2)$ : Since an  $N$ -vertex graph  $G_{\mathbf{a}}$  with  $N < m$  cannot contain an  $m$ -clique, it follows that  $C_m^N(\mathbf{a}) = 0$  for all such  $G_{\mathbf{a}}$ . Thus, for  $N < m$ ,  $h_{m,2}^N(\mathbf{a}) = I_2^N(\mathbf{a}) = \bar{a}_1 + \dots + \bar{a}_{L_N}$ , where  $\bar{a}_i = 1 - a_i$ . This produces a problem Hamiltonian  $H_P$  with  $L_N$  uncoupled qubits which is easily mapped onto the chip. Now consider  $N = m$ . Defining  $L = L_m = \binom{m}{2}$ , we have  $C_m^m(\mathbf{a}) = a_1 a_2 \dots a_{L-1} a_L$ , and  $h_{m,2}^m(\mathbf{a}) = C_m^m(\mathbf{a}) + I_2^m(\mathbf{a})$ . The  $L$ -bit interaction in  $C_m^m(\mathbf{a})$  is reduced to pairwise coupling by introducing: (i) ancillary bit variables  $b_2, \dots, b_{L-1}$ , and (ii) imposing the constraints  $b_{L-1} = a_{L-1} a_L$  and  $b_j = a_j b_{j+1}$  ( $j = 2, \dots, L-2$ ) through the penalty function  $P(\mathbf{a}; \mathbf{b}) = P(a_{L-1}, a_L; b_{L-1}) + \sum_{j=2}^{L-2} P(a_j, b_{j+1}; b_j)$ , where  $P(a, b; c)$  was defined in Section 2(a). The  $R(m, 2)$  cost function for  $N = m$  is then  $h_{m,2}^m(\mathbf{a}, \mathbf{b}) = \{a_1 b_2 + \mu P(\mathbf{a}; \mathbf{b})\} + I_2^m(\mathbf{a})$ , where  $\mu = 2$  is the penalty weight value used in all  $R(m, 2)$  experiments. Making the substitutions  $2\mathbf{a} = \mathbf{s}_a + 1$  and  $2\mathbf{b} = \mathbf{s}_b + 1$  expresses the cost function in terms of Ising spin variables  $\mathbf{s}_a$  and  $\mathbf{s}_b$ . The PG for the pairwise interactions present in  $h_{m,2}^m(\mathbf{a}, \mathbf{b})$  appears in the SI. We have embedded this PG into the hardware up to  $N = m = 8$ . In the SI we display the embedding that was used to determine  $R(8, 2)$  which used 28 computational qubits, 26 ancilla qubits to reduce interactions to pairwise, and 30 qubits to match the PG connectivity to the qubit connectivity available on the chip for a total of 84 qubits.

(b)  $R(3, 3)$ : We also determined  $R(3, 3)$  by examining  $N = 4, 5, 6$ . The cost functions for these cases are:

$$\begin{aligned} h_{3,3}^4(\mathbf{a}) &= f_{1,2,4} + f_{1,3,5} + f_{2,3,6} + f_{4,5,6}; \\ h_{3,3}^5(\mathbf{a}) &= f_{1,2,5} + f_{1,3,6} + f_{1,4,7} + f_{2,3,8} + f_{2,4,9} + \\ &\quad f_{3,4,10} + f_{5,6,8} + f_{5,7,9} + f_{6,7,10} + f_{8,9,10}; \\ h_{3,3}^6(\mathbf{a}) &= f_{1,2,6} + f_{1,3,7} + f_{1,4,8} + f_{1,5,9} + f_{2,3,10} + f_{2,4,11} \\ &\quad + f_{2,5,12} + f_{3,4,13} + f_{3,5,14} + f_{4,5,15} + f_{6,7,10} \\ &\quad + f_{6,8,11} + f_{6,9,12} + f_{7,8,13} + f_{7,9,14} + f_{8,9,15} \\ &\quad + f_{10,11,13} + f_{10,12,14} + f_{11,12,15} + f_{13,14,15}; \end{aligned}$$

where  $f_{i,j,k} = a_i a_j a_k + \bar{a}_i \bar{a}_j \bar{a}_k$ . Notice that  $f_{i,j,k}$  can be re-written as  $f_{i,j,k} = -2 + \bar{a}_i + \bar{a}_j + \bar{a}_k + a_i a_j + a_i a_k + a_j a_k$ , which only contains pairwise couplings, making ancillary  $\mathbf{b}$ -qubits unnecessary. The largest of these problems is for  $N = 6$  whose PG has 15 vertices and 60 edges.

We can reduce its size slightly by exploiting the identity  $h_{m,n}^N(\mathbf{a}) = h_{n,m}^N(\bar{\mathbf{a}})$ . For  $m = n$  this yields a two-fold symmetry: if  $\mathbf{a}_*$  is a global minimum of  $h_{m,m}^N$ , so is  $\bar{\mathbf{a}}_*$ . Thus, we can fix one variable (say  $a_1 = 0$ ) and optimize over the remaining variables  $\mathbf{a}'$ . Optimal solutions then have the form  $(0, \mathbf{a}'_*)$  and  $(1, \bar{\mathbf{a}}'_*)$ . With this simplification, the PG of  $h_{3,3}^6(0, \mathbf{a}')$  has 14 vertices and 52 edges. We show its embedding into the chip hardware in the SI.

**4. Results:** To solve a given Ramsey COP specified by the parameters  $\mathbf{h}$  and  $\mathbf{J}$ , the chip must first be programmed to fix these values in hardware. For the largest problem we solved ( $R(8, 2)$  using 84 qubits) this took roughly 270 ms. After programming we iterate many cycles of annealing and readout. Each annealing cycle has duration  $t_f = 1$  ms, and readout of the qubits takes 1.5 ms per sample. Programming only occurs once so the total runtime required to obtain  $S$  Ramsey output samples is  $270 + (1 + 1.5)S$  ms. As the hardware is an analog device, there is limited precision to which  $\mathbf{h}$  and  $\mathbf{J}$  can be specified. For a COP whose ground state is sensitive to parameter settings this could pose serious difficulties. However, the Ramsey COP requires specification of only a few distinct integral values, and ground states are quite stable to parameter perturbations. The reader is referred to the SI for further discussion of: (i) the quantum annealing rate and the distribution of final energies; (ii) the experimental temperature; and (iii) parameter noise.

Figs. 1 and 3 present our results for  $R(8, 2)$  and  $R(3, 3)$ . Due to space limitations, our full set of results ( $R(3, 3)$  and  $R(m, 2)$  with  $4 \leq m \leq 8$ ) appear in the SI, though Table I contains a summary of all results, along with corresponding theoretical predictions. Both Figures 1 and 3 display histograms that plot the relative-frequency of energy values obtained by programming the chip and running  $10^5$  annealing and readout cycles, yielding  $10^5$   $\mathbf{s}$ -spin configurations. In the main figures, histograms of the energies of the Ising problem sent to the hardware are plotted. These Ising cost functions include the Ramsey cost function  $h_{m,n}^N(\mathbf{s})$ , and the ferromagnetic penalties,  $\lambda$ , enforcing the equality constraints amongst qubits that represent the same PG spin variable. The ferromagnetic penalty weight used for embedding was adjusted so that at least 85% of output  $\mathbf{s}$ -configurations satisfied the equality constraints. These feasible spin configurations were translated back to the original  $\mathbf{a}$  variables and the cost/energy function  $h_{m,n}^N(\mathbf{a})$  evaluated. The resulting energy values were binned and plotted in the inset histograms. Further discussion of the equality constraint protocol appears in the SI.

Fig. 1 presents our results for  $R(8, 2)$  for  $N = 7$  and 8, while  $N = 6$  appears in the SI. The  $R(8, 2)$  experiment was the largest of the  $R(m, 2)$  problems considered. Of the  $\mathbf{s}$ -configurations returned by the hardware for  $N = 8$ , approximately 65% are global minima of  $h_{8,2}^8$ . By comparison, steepest-descent local-search started from a random spin configuration finds a globally minimal configuration with less than 0.01% probability. Note that classical/thermal annealing can be ruled out as the source

TABLE I: Results for Ramsey numbers  $R(m, 2) = m$  for  $4 \leq m \leq 8$ , and  $R(3, 3) = 6$ . Here  $N$  is the number of graph vertices;  $E_{gs}$  and  $D$  are the ground-state energy and degeneracy, respectively, for the problem Hamiltonian  $H_P$ ; and for each Ramsey number, the experimental results are followed by the theoretical predictions from Ref. 3 in parenthesis.

R(2, 4)			R(2, 5)			R(2, 6)			R(2, 7)			R(2, 8)			R(3, 3)		
$N$	$E_{gs}$	$D$	$N$	$E_{gs}$	$D$	$N$	$E_{gs}$	$D$	$N$	$E_{gs}$	$D$	$N$	$E_{gs}$	$D$	$N$	$E_{gs}$	$D$
3	0(0)	1(1)	4	0(0)	1(1)	5	0(0)	1(1)	6	0(0)	1(1)	7	0(0)	1(1)	5	0(0)	12(12)
4	1(1)	7(7)	5	1(1)	11(11)	6	1(1)	16(16)	7	1(1)	22(22)	8	1(1)	29(29)	6	2(2)	1758(1760)

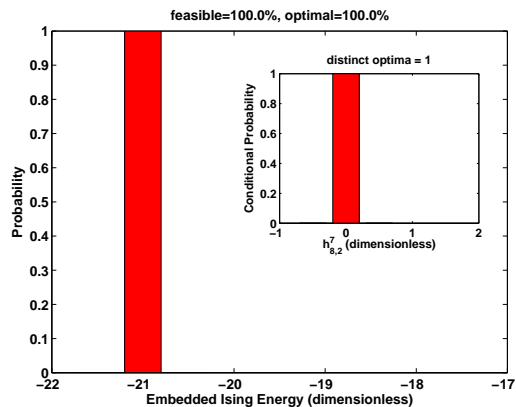
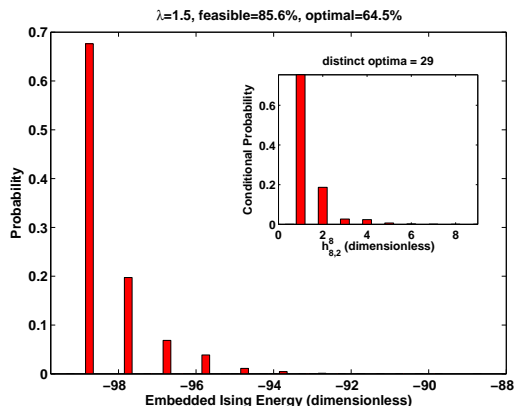
(a)  $N = 7$ (b)  $N = 8$ 

FIG. 1: Energy histograms for  $R(8, 2)$  on graphs below ( $N = 7$ ) and at ( $N = 8$ ) the Ramsey transition.

of optimization efficacy. First, it is clear that the hardware is not realizing classical annealing since the final distribution of low energy states is not Boltzmann distributed as discussed in the SI, Sec. VI B, and furthermore, the temperature of the hardware is never varied during the experiments. Finally, we compare the optimization efficacy of the hardware with that of an efficient C-implementation of simulated annealing that was run on a standard 8Gb, 2.66GHz desktop computer. The results of Fig. 2 show that at a runtime of  $2.5ms$  (which is the  $1ms$  runtime plus  $1.5ms$  read-out time of the Ramsey

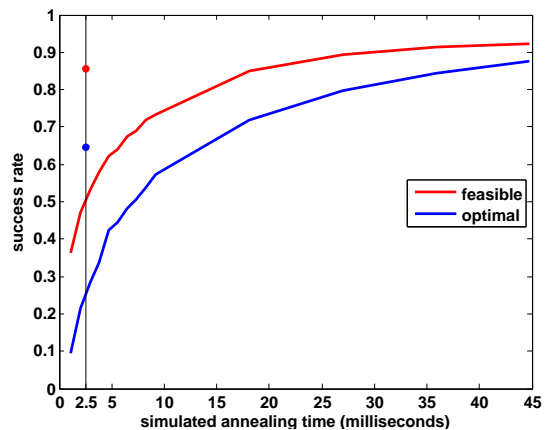


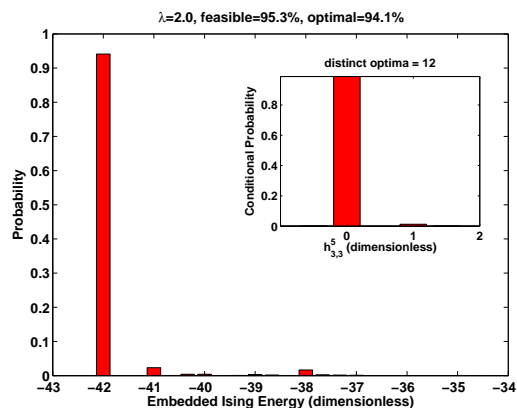
FIG. 2: Plot of simulated annealing (SA) success probability to determine optimal and feasible spin-configurations versus run-time for  $R(8, 2)$  at  $N = 8$ . The SA cooling schedule is exponential; and the initial and final temperatures were optimized for maximum success probability. For comparison, the D-Wave hardware results are also shown for a runtime of  $2.5ms$ . See text for further discussion.

number experiments), the hardware obtains significantly higher success rates for finding both feasible and optimal final spin-configurations than does simulated annealing. Returning to Fig. 1, examination of the inset histograms for  $N = 7$  (8) we see that: (i)  $h_{min} = 0$  (1); (ii) the probability for  $h = 0$  (1) is approximately 1.0 (0.65); and (iii) the number of optimal  $\mathbf{a}$ -configurations/graphs is 1 (29). The reader is referred to the SI for an explanation of how the probability for an optimal spin-configuration is determined. The energies  $h_{min}$  found for  $N = 7$  and 8 agree with the final ground-state (GS) energies found in Ref. 3, indicating that the hardware finds the final GS with high-probability. As  $h_{min}$  jumps from  $0 \rightarrow 1$  as  $N$  goes from  $7 \rightarrow 8$ , the Ramsey protocol correctly<sup>5</sup> identifies  $R(8, 2) = 8$ . Finally, Ref. 3 showed that the number of optimal graphs for  $N = 7$  (8) is 1 (29) which agrees with what was found by the hardware. For  $N = 7$ , the unique optimal  $\mathbf{a}$ -configuration corresponds to the graph in which every pair of vertices is connected by an edge and so has no 2-independent sets or 8-clique and so has  $h_{8,2}^7 = 0$ . For  $N = 8$ , the 29 optimal  $\mathbf{a}$ -configurations correspond to graphs  $G_{\mathbf{a}}$  with  $h_{8,2}^8(\mathbf{a}) = 1$  which are the 28 eight-vertex graphs containing a single 2-independent

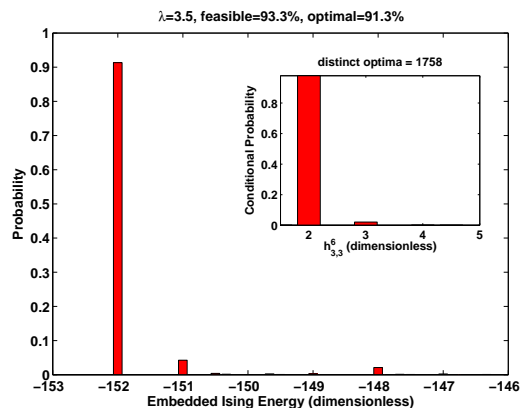


set, and the single 8-vertex graph containing an 8-clique.

Fig. 3 shows our results for  $R(3, 3)$  with  $N = 5$  and



(a)  $N = 5$



(b)  $N = 6$

FIG. 3: **Energy histograms for  $R(3, 3)$**  on graphs below ( $N = 5$ ) and at ( $N = 6$ ) the Ramsey transition.

6, while  $N = 4$  appears in the SI. Together, they show that the minimum energies for  $N = 4, 5, 6$  are 0, 0, 2, respectively, and these occur with probabilities of approx-

imately 93%, 94%, and 91%. These success rates are much higher than steepest-descent local-search. The success rate for randomly initialized local search is less than 1% for  $N = 6$ . The energies  $h_{min}$  agree with the final GS energies found in Ref. 3 indicating that the hardware again finds the final GS with high-probability. As  $h_{min}$  jumps from  $0 \rightarrow 2$  as  $N$  goes from  $5 \rightarrow 6$ , the Ramsey protocol correctly<sup>5</sup> identifies  $R(3, 3) = 6$ . Finally, Ref. 3 showed that the number of optimal graphs for  $N = 4, 5, 6$  is 18, 12, 1760, respectively, in excellent agreement with the hardware results of 18, 12, 1758.

**5. Discussion:** We presented results of an experimental implementation of the RNA<sup>3</sup>. As the Ramsey numbers found correspond to known Ramsey numbers, it was possible to validate RNA performance. Agreement between theory and experiment was excellent: experimental implementation of the RNA correctly determined: (i)  $R(m, 2) = m$  for  $4 \leq m \leq 8$  and  $R(3, 3) = 6$ ; and (ii) the corresponding final ground-state energies and degeneracies. Our results provide evidence of a quantum implementation of the RNA based on adiabatic evolution. Further evidence that the D-Wave hardware implements quantum annealing has recently been reported<sup>12</sup>. It was argued in Ref. 13 that this evidence did not imply quantum annealing, though these arguments were refuted in Ref. 14. Finally, we stress that the optimization formulations necessary for experimental realization of the RNA were non-trivial. The Ising problems after embedding, solved with high success rate by the hardware, have many local minima which were responsible for the low success rates of iterated local-search. In spite of the many local minima, the hardware implementation of the RNA correctly determined all of the above Ramsey numbers. The  $R(8, 2)$  computation used 84 qubits of which 28 were computational qubits, and to the best of our knowledge is the largest experimental implementation of a scientifically meaningful adiabatic evolution algorithm.

**Acknowledgements** We thank the D-Wave hardware team for providing this experimental platform, and M. Amin, R. Harris, T. Lanting, and M. Thom for valuable suggestions. F. G. thanks T. Howell III for continued support.

<sup>1</sup> Vandersypen, L.M.K. et al., *Nature* **414**, 883 (2001).

<sup>2</sup> Xu, N. et al., *Phys. Rev. Lett.* **108**, 130501 (2012).

<sup>3</sup> Gaitan, F. & Clark, L., *Phys. Rev. Lett.* **108**, 010501 (2012).

<sup>4</sup> Graham, R. L., Rothschild, B. L., & Spencer, J. H., *Ramsey Theory* (John Wiley & Sons, New York, 1990).

<sup>5</sup> Bollobás, B., *Modern Graph Theory* (Springer, New York, 1998).

<sup>6</sup> Farhi, E., Goldstone, J., Gutmann, S., & Sipser, M., <http://arxiv.org/abs/quant-ph/0001106> (2000).

<sup>7</sup> T. Kadowaki and H. Nishimori, *Phys. Rev. E* **58**, 5355

(1998); G. E. Santoro et al. *Science* **295**, 2427 (2002).

<sup>8</sup> Harris, R. et al., *Phys. Rev. B* **81**, 134510 (2010).

<sup>9</sup> Harris, R. et al., *Phys. Rev. B* **80**, 052506 (2009).

<sup>10</sup> Harris, R. et al., *Phys. Rev. B* **82**, 024511 (2010).

<sup>11</sup> Johnson, M. W. et al., *Nature* **473**, 194 (2011).

<sup>12</sup> Boixo et al., *Nature Comm.* **4**, 2067 (2013); Boixo et al., arXiv:1304.4595.

<sup>13</sup> J.A. Smolin and G. Smith, arXiv:1305.4904.

<sup>14</sup> Wang et al., arXiv:1305.5837.

# Supporting Information for “Experimental determination of Ramsey numbers”

Zhengbing Bian,<sup>1</sup> Fabian Chudak,<sup>1</sup> William G. Macready,<sup>1</sup> Lane Clark,<sup>2</sup> and Frank Gaitan<sup>3</sup>

<sup>1</sup>*D-Wave Systems, Inc., 100-4401 Still Creek Drive, Burnaby, British Columbia V5C 6G9, Canada*

<sup>2</sup>*Department of Mathematics, Southern Illinois University, Carbondale, IL 62901-4401*

<sup>3</sup>*Laboratory for Physical Sciences, 8050 Greenmead Dr, College Park, MD 20740*

(Dated: November 1, 2018)

In this supplement we briefly review the construction of the Ramsey number quantum algorithm, and discuss its experimental implementation. We then present the complete set of Ramsey number experimental results, including those that could not be included in the manuscript due to space limitations. Next we present two examples of embeddings of the Ramsey problem Hamiltonian  $H_P$  into the chip hardware. These embeddings explicitly show how qubit couplings are laid out on the chip so as to reproduce the couplings appearing in the problem Hamiltonian  $H_P$ . Finally, we close with a discussion of a number of important issues associated with the Ramsey number experiments and their analysis.

PACS numbers: 03.67.Ac,02.10.Ox,89.75.Hc

The structure of this Supporting Information (SI) is as follows. We begin in Section I with a description of how the Ramsey number quantum algorithm is constructed, and then discuss its experimental implementation in Sections II and III. Section IV then presents the complete set of Ramsey number experimental results, including those that could not be included in the manuscript due to space limitations. Section IV A presents the results for  $R(3,3)$ , while Section IV B presents the results for the Ramsey numbers  $R(m,2)$  with  $4 \leq m \leq 8$ . For easy reference, Section IV A and Section IV B also include the data for  $R(3,3)$  with  $N = 5$  and  $6$ , and  $R(8,2)$  for  $N = 7$  and  $8$ , respectively, which appear in Section 4 of the manuscript. Section V displays the embedding of the Ramsey energy functions into the chip for  $R(3,3)$  with  $N = 6$  (Section V C) and  $R(8,2)$  with  $N = 8$  (Section V A). These embeddings represent the most complex embeddings we encountered in our experimental determination of, respectively, diagonal ( $R(m,m)$ ) and non-diagonal ( $R(m,n)$ ,  $m \neq n$ ) Ramsey numbers. Finally, we close in Section VI with a discussion of a number of important issues associated with the Ramsey number experiments and their analysis.

## I. RAMSEY NUMBER QUANTUM ALGORITHM

We briefly describe the Ramsey number quantum adiabatic algorithm (see Ref. 1 for details). We begin by establishing a 1-1 correspondence between the set of  $N$ -vertex graphs and binary strings of length  $L = N(N-1)/2$ . To each  $N$ -vertex graph  $G$  there corresponds a unique adjacency matrix  $A(G)$  which is an  $N \times N$  symmetric matrix with vanishing diagonal matrix elements, and with off-diagonal element  $a_{i,j} = 1$  ( $0$ ) when distinct vertices  $i$  and  $j$  are (are not) joined by an edge. It follows that  $A(G)$  is determined by its lower triangular part. By concatenating column-wise the matrix elements  $a_{i,j}$  appearing below the principal diagonal, we can construct a unique binary string  $g(G)$  of length  $L$  for each graph  $G$ :

$$g(G) \equiv a_{2,1} \cdots a_{N,1} a_{3,2} \cdots a_{N,2} \cdots a_{N,N-1}. \quad (1)$$

Given the string  $g(G)$ , the following procedure determines the number of  $m$ -cliques in  $G$ . Choose  $m$  vertices,  $S_\alpha = \{v_1, \dots, v_m\}$ , from the  $N$  vertices of  $G$  and form the product  $\mathcal{C}_\alpha = \prod_{\substack{j \neq k \\ (v_j, v_k \in S_\alpha)}} a_{v_j, v_k}$ . Note that  $\mathcal{C}_\alpha = 1$  when  $S_\alpha$  forms an  $m$ -clique; otherwise  $\mathcal{C}_\alpha = 0$ . Now repeat this procedure for all  $\rho = \binom{N}{m}$  ways of choosing  $m$  vertices from  $N$  vertices, and form the sum  $\mathcal{C}_m^N(G) = \sum_{\alpha=1}^{\rho} \mathcal{C}_\alpha$ . By construction,  $\mathcal{C}_m^N(G)$  equals the number of  $m$ -cliques contained in  $G$ . A similar procedure determines the number of  $n$ -independent sets in  $G$ . Briefly, choose  $n$  vertices  $T_\alpha = \{v_1, \dots, v_n\}$  from the  $N$  vertices in  $G$ , and form the product  $\mathcal{I}_\alpha = \prod_{\substack{j \neq k \\ (v_j, v_k \in T_\alpha)}} \bar{a}_{v_j, v_k}$ , where  $\bar{a}_{v_j, v_k} = 1 - a_{v_j, v_k}$ . Note that if  $\mathcal{I}_\alpha = 1$ , then  $T_\alpha$  forms an  $n$ -independent set; otherwise  $\mathcal{I}_\alpha = 0$ . Repeat this for all  $\nu = \binom{N}{n}$  ways of choosing  $n$  vertices from  $N$  vertices, then form the sum  $\mathcal{I}_n^N(G) = \sum_{\alpha=1}^{\nu} \mathcal{I}_\alpha$ . By construction,  $\mathcal{I}_n^N(G)$  gives the number of  $n$ -independent sets contained in  $G$ . Finally, define

$$h_{m,n}^N(G) = \mathcal{C}_m^N(G) + \mathcal{I}_n^N(G). \quad (2)$$

It follows from the above discussion that  $h_{m,n}^N(G)$  is the total number of  $m$ -cliques and  $n$ -independent sets in  $G$ . Thus  $h_{m,n}^N(G) \geq 0$  for all graphs  $G$ ; and  $h_{m,n}^N(G) = 0$  if and only if  $G$  does not contain an  $m$ -clique or  $n$ -independent set.

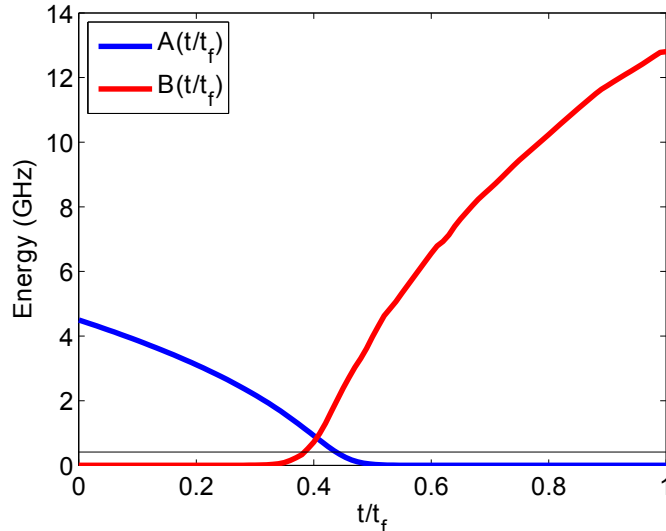


FIG. 1: **Interpolation functions**  $A(t/t_f)$  and  $B(t/t_f)$ . The functional forms of the experimentally measured interpolation functions  $A(t/t_f)$  and  $B(t/t_f)$  are shown. The QA run-time  $t_f$  can be adjusted for times ranging from 20–20 000  $\mu\text{s}$ . For comparison, the temperature at which the experiment is performed is shown as the line at roughly 0.4 GHz.

We use  $h_{m,n}^N(G)$  as the cost function for the following combinatorial optimization problem. For given integers  $N$ ,  $m$  and  $n$ , and with  $h_{m,n}^N(G)$  defined as above, find an  $N$ -vertex graph  $G_*$  that yields the global minimum of  $h_{m,n}^N(G)$ . Notice that if  $N < R(m, n)$ , the (global) minimum will be  $h_{m,n}^N(G_*) = 0$  since Ramsey theory guarantees that a graph exists which has no  $m$ -clique or  $n$ -independent set. On the other hand, if  $N \geq R(m, n)$ , Ramsey theory guarantees  $h_{m,n}^N(G_*) > 0$ . If we begin with  $N < R(m, n)$  and increment  $N$  by 1 until we first find  $h_{m,n}^N(G_*) > 0$ , then the corresponding  $N$  will be exactly  $R(m, n)$ . We now show how this combinatorial optimization problem can be solved using adiabatic quantum evolution, which then becomes the basis for a quantum algorithm to compute  $R(m, n)$ .

The adiabatic quantum evolution (AQE) algorithm [2] exploits the adiabatic dynamics of a quantum system to solve combinatorial optimization problems. The AQE algorithm uses the optimization problem cost function to define a problem Hamiltonian  $H_P$  whose ground-state eigenspace encodes all problem solutions. The algorithm evolves the state of an  $L$ -qubit register from the ground-state of an initial Hamiltonian  $H_i$  to the ground-state of  $H_P$  with probability approaching 1 in the adiabatic limit. An appropriate measurement at the end of the adiabatic evolution yields a solution of the optimization problem almost certainly. The time-dependent Hamiltonian  $H(t)$  for local AQE is

$$H(t) = A(t/t_f)H_i + B(t/t_f)H_P, \quad (3)$$

where  $t_f$  is the algorithm run-time; adiabatic dynamics corresponds to  $t_f \rightarrow \infty$ ; and  $A(t/t_f)$  ( $B(t/t_f)$ ) is a positive monotonically decreasing (increasing) function with  $A(1) = 0$  ( $B(0) = 0$ ). The experimentally measured functional forms of the interpolation functions  $A(t/t_f)$  and  $B(t/t_f)$  are shown in Fig. 1.

To map the optimization problem associated with computing  $R(m, n)$  onto an adiabatic quantum computation, we begin with the 1-1 correspondence between  $N$ -vertex graphs  $G$  and length  $L = N(N-1)/2$  binary strings  $g(G)$ . From Eq. (1) we see that position along the string is indexed by the graph edges  $(i, j)$ . We thus identify a qubit with each vertex pair  $(i, j)$ , and will thus need  $L$  qubits. Defining the computational basis states (CBS) to be the eigenstates of  $\sigma_z^0 \otimes \dots \otimes \sigma_z^{L-1}$ , we identify the  $2^L$  graph strings  $g(G)$  with the  $2^L$  CBS:  $g(G) \rightarrow |g(G)\rangle$ . The problem Hamiltonian  $H_P$  is defined to be diagonal in the computational basis with eigenvalue  $h_{m,n}^N(G)$  associated with eigenstate  $|g(G)\rangle$ :

$$H_P|g(G)\rangle = h_{m,n}^N(G)|g(G)\rangle. \quad (4)$$

Note that the ground-state energy of  $H_P$  will be zero iff there is a graph with no  $m$ -cliques or  $n$ -independent sets. An operator expression for  $H_P$  appears in Ref. 1. The initial Hamiltonian  $H_i$  is chosen to be

$$H_i = - \sum_{i=0}^{L-1} \sigma_x^i, \quad (5)$$

where  $I^i$  and  $\sigma_x^i$  are, respectively, the identity and x-Pauli operator for qubit  $i$ . The ground-state of  $H_i$  is the easily constructed uniform superposition of CBS[2].

The quantum algorithm for computing  $R(m, n)$  begins by setting  $N$  equal to a strict lower bound for  $R(m, n)$  which can be found using the probabilistic method [3] or a table of two-color Ramsey numbers [6]. The AQE algorithm is run on  $L_N = N(N - 1)/2$  qubits, and the energy  $E$  is measured at the end of algorithm execution. In the adiabatic limit the result will be  $E = 0$  since  $N < R(m, n)$ . The value of  $N$  is incremented  $N \rightarrow N + 1$ , the AQE algorithm is re-run on  $L_{N+1}$  qubits, and the energy is measured at the end of algorithm execution. This process is repeated until  $E > 0$  first occurs, at which point the current value of  $N$  will be equal to the  $R(m, n)$ . Note that any real application of AQE will only be approximately adiabatic. Thus the probability that the measured energy  $E$  will be the ground-state energy will be  $1 - \epsilon$ . In this case, the algorithm must be run  $k \sim \mathcal{O}(\ln[1 - \delta]/\ln \epsilon)$  times so that, with probability  $\delta > 1 - \epsilon$ , at least one of the measurement outcomes will be the true ground-state energy. We can make  $\delta$  arbitrarily close to 1 by choosing  $k$  sufficiently large.

Although most discussions of QA assume zero-temperature, all experiments here were performed at 20 mK, or roughly 0.4 GHz. For comparison, peak values of the interpolation functions  $A(t/t_f)$  and  $B(t/t_f)$  are of order 10 GHz (see Fig. 1). Refs. 4 and 5 showed that finite temperature need not destroy the efficacy of QA. In our experiments we select the lowest energy configuration observed over many annealing cycles to compensate for the stochastic influence of non-zero temperature.

## II. EXPERIMENTAL IMPLEMENTATION OF RAMSEY COST FUNCTIONS

To match the notation used in the manuscript we make the substitution  $g(G) \rightarrow \mathbf{a}$  in Eq. (1) and write the Ramsey cost function as  $h_{m,n}^N(\mathbf{a})$ . The cost function  $h_{m,n}^N(\mathbf{a})$  is not yet ready for experimental implementation for two reasons: (a) there are  $k$ -qubit interactions with  $k > 2$ ; and (b) the qubit couplings do not correspond to the qubit couplings in Fig. 2. These obstacles are removed as follows.

(a) *Reduction to pairwise coupling*: Section I above showed that  $C_m^N(\mathbf{a})$  involves interactions coupling  $\binom{m}{2}$  qubits, while  $I_n^N(\mathbf{a})$  couples  $\binom{n}{2}$  qubits. These interactions must be reduced to pairwise coupling if  $h_{m,n}^N(\mathbf{a})$  is to be realized experimentally. We illustrate how such a reduction can be achieved by reducing the 3-bit coupling term  $a_1 a_2 a_3$  to pairwise coupling using an ancillary bit-variable  $b$  and penalty function

$$P(a_1, a_2; b) = a_1 a_2 - 2(a_1 + a_2)b + 3b. \quad (6)$$

Notice that  $P(a_1, a_2; b) = 0$  ( $> 0$ ) when the input values for  $a_1$ ,  $a_2$ , and  $b$  satisfy  $b = a_1 a_2$  ( $b \neq a_1 a_2$ ). Now consider the quadratic cost function  $h(b) = b a_3 + \mu P(a_1, a_2; b)$  for given values of  $\mu$  and  $a_i$ . For  $\mu$  sufficiently large,  $h(b)$  is minimized when  $b$  satisfies the equality constraint  $b = a_1 a_2$  which causes the penalty function to vanish. The optimum cost is then  $h(b = a_1 a_2) = a_1 a_2 a_3$  which reproduces the 3-bit coupling term using a *quadratic* cost function. This example is generalized in Sec. 3 to produce the quadratic cost function used to calculate  $R(m, 2)$ .

(b) *Matching spin to qubit connectivity*: A cost function with only pairwise qubit coupling may still not be experimentally realizable as the qubit couplings needed may not match the qubit couplings available on chip. The primal graph (PG) of a quadratic cost function is the graph whose vertices are the qubit variables, and whose edges indicate pairwise-coupled qubits. An arbitrary PG can be embedded into a sufficiently large qubit graph having the structure of Fig. 2. An embedding maps a PG vertex to one or more vertices in the qubit graph, where the image vertices form a connected subgraph of the qubit graph. We link this connected set of qubits together with strong ferromagnetic couplings so that in the lowest energy state these qubits have identical Bloch vectors. For example, to couple qubits 104 and 75 in Fig. 2 (which are not directly coupled) with coupling strength  $\mathcal{J}$ , we ferromagnetically couple qubits 104, 112, and 107 using strongly negative  $J_{104,112}$  and  $J_{107,112}$  values. The desired coupling is then carried along the edge connecting qubits 107 and 75 with  $J_{75,107} = \mathcal{J}$ .

## III. RAMSEY ENERGY FUNCTIONS

We examined a number of Ramsey problems which could be solved using the 106 qubits available in Fig. 2. Specifically,  $R(m, 2)$  with  $4 \leq m \leq 8$  and  $R(3, 3)$ .

(a)  $R(m, 2)$ : Since an  $N$ -vertex graph  $G_{\mathbf{a}}$  with  $N < m$  cannot contain an  $m$ -clique, it follows that  $C_m^N(\mathbf{a}) = 0$  for all such  $G_{\mathbf{a}}$ . Thus, for  $N < m$ ,  $h_{m,2}^N(\mathbf{a}) = I_2^N(\mathbf{a}) = \bar{a}_1 + \dots + \bar{a}_N$ , where  $\bar{a}_i = 1 - a_i$ . This produces a problem Hamiltonian  $H_P$  with  $L_N$  *uncoupled* qubits which is easily mapped onto the chip. Now consider  $N = m$ . Defining  $L = L_m = \binom{m}{2}$ , we have  $C_m^m(\mathbf{a}) = a_1 a_2 \dots a_{L-1} a_L$ , and  $h_{m,2}^m(\mathbf{a}) = C_m^m(\mathbf{a}) + I_2^m(\mathbf{a})$ . The  $L$ -bit interaction in  $C_m^m(\mathbf{a})$  is reduced to pairwise coupling by introducing: (i) ancillary bit variables  $b_2, \dots, b_{L-1}$ , and (ii) imposing the constraints  $b_{L-1} = a_{L-1} a_L$



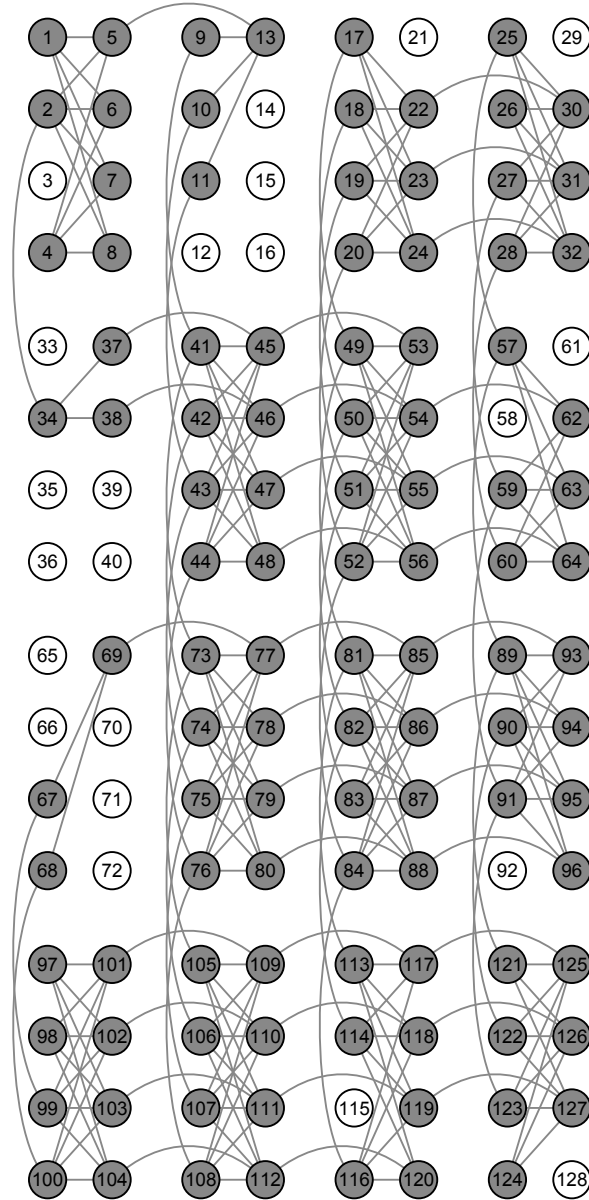


FIG. 2: **Layout of qubits and couplers.** The chip architecture is a  $4 \times 4$  array of unit cells, with each unit cell containing 8 qubits. Within a unit cell, each of the 4 qubits in the left-hand partition (LHP) connects to all 4 qubits in the right-hand partition (RHP), and vice versa. A qubit in the LHP (RHP) of a unit cell also connects to the corresponding qubit in the LHP (RHP) in the units cells above and below (to the left and right of) it. Most qubits couple to 6 neighbors. Qubits are labeled from 1 to 128, and edges between qubits indicate couplers which may take programmable values. Grey qubits indicate usable qubits, while white qubits indicate qubits which, due to fabrication defects, could not be calibrated to operating tolerances and were not used. All experiments were done on a chip with 106 usable qubits.

and  $b_j = a_j b_{j+1}$  ( $j = 2, \dots, L-2$ ) through the penalty function  $P(\mathbf{a}; \mathbf{b}) = P(a_{L-1}, a_L; b_{L-1}) + \sum_{j=2}^{L-2} P(a_j, b_{j+1}; b_j)$  (see Eq. (6)). The  $R(m, 2)$  cost function for  $N = m$  is then  $h_{m,2}^m(\mathbf{a}, \mathbf{b}) = \{a_1 b_2 + \mu P(\mathbf{a}; \mathbf{b})\} + I_2^m(\mathbf{a})$ , where  $\mu = 2$  is the penalty weight value used in all  $R(m, 2)$  experiments. Making the substitutions  $2\mathbf{a} = \mathbf{s}_a + 1$  and  $2\mathbf{b} = \mathbf{s}_b + 1$  expresses the cost function in terms of Ising spin variables  $\mathbf{s}_a$  and  $\mathbf{s}_b$ . The PG for the pairwise interactions present in  $h_{m,2}^m(\mathbf{a}, \mathbf{b})$  appears in Figure 9. We have embedded this PG into the hardware up to  $N = m = 8$ . In Fig. 10 we display the embedding that was used to determine  $R(8, 2)$  which used 28 computational qubits, 26 ancilla qubits to reduce interactions to pairwise, and 30 qubits to match the PG connectivity to the qubit connectivity in Fig. 10 for a total of 84 qubits.

TABLE I: Results<sup>1</sup> for Ramsey numbers  $R(m, 2) = m$  for  $4 \leq m \leq 8$  and  $R(3, 3) = 6$ .

<b>R(2, 4)</b>			<b>R(2, 5)</b>			<b>R(2, 6)</b>			<b>R(2, 7)</b>			<b>R(2, 8)</b>			<b>R(3, 3)</b>		
$N$	$E_{gs}$	$D$	$N$	$E_{gs}$	$D$	$N$	$E_{gs}$	$D$	$N$	$E_{gs}$	$D$	$N$	$E_{gs}$	$D$	$N$	$E_{gs}$	$D$
3	0(0)	1(1)	4	0(0)	1(1)	5	0(0)	1(1)	6	0(0)	1(1)	7	0(0)	1(1)	5	0(0)	12(12)
4	1(1)	7(7)	5	1(1)	11(11)	6	1(1)	16(16)	7	1(1)	22(22)	8	1(1)	29(29)	6	2(2)	1758(1760)

<sup>1</sup> $N$  is the number of graph vertices;  $E_{gs}$  and  $D$  are the ground-state energy and degeneracy, respectively, for the problem Hamiltonian  $H_P$ ; and for each Ramsey number, the experimental results are followed by the theoretical predictions from Ref. 1 in parenthesis.

(b)  $R(3, 3)$ : We also determined  $R(3, 3)$  by examining  $N = 4, 5, 6$ . The cost functions for these cases are:

$$\begin{aligned}
h_{3,3}^4(\mathbf{a}) &= f_{1,2,4} + f_{1,3,5} + f_{2,3,6} + f_{4,5,6}; \\
h_{3,3}^5(\mathbf{a}) &= f_{1,2,5} + f_{1,3,6} + f_{1,4,7} + f_{2,3,8} + f_{2,4,9} + \\
&\quad f_{3,4,10} + f_{5,6,8} + f_{5,7,9} + f_{6,7,10} + f_{8,9,10}; \\
h_{3,3}^6(\mathbf{a}) &= f_{1,2,6} + f_{1,3,7} + f_{1,4,8} + f_{1,5,9} + f_{2,3,10} + f_{2,4,11} \\
&\quad + f_{2,5,12} + f_{3,4,13} + f_{3,5,14} + f_{4,5,15} + f_{6,7,10} \\
&\quad + f_{6,8,11} + f_{6,9,12} + f_{7,8,13} + f_{7,9,14} + f_{8,9,15} \\
&\quad + f_{10,11,13} + f_{10,12,14} + f_{11,12,15} + f_{13,14,15};
\end{aligned}$$

where  $f_{i,j,k} = a_i a_j a_k + \bar{a}_i \bar{a}_j \bar{a}_k$ . Notice that  $f_{i,j,k}$  can be re-written as  $f_{i,j,k} = -2 + \bar{a}_i + \bar{a}_j + \bar{a}_k + a_i a_j + a_i a_k + a_j a_k$ , which only contains *pairwise* couplings, making ancillary  $\mathbf{b}$ -qubits unnecessary. The largest of these problems is  $N = 6$  whose PG has 15 vertices and 60 edges. We can reduce its size slightly by exploiting the identity  $h_{m,n}^N(\mathbf{a}) = h_{n,m}^N(\bar{\mathbf{a}})$ . For  $m = n$  this yields a two-fold symmetry: if  $\mathbf{a}_*$  is a global minimum of  $h_{m,m}^N$ , so is  $\bar{\mathbf{a}}_*$ . Thus, we can fix one variable (say  $a_1 = 0$ ) and optimize over the remaining variables  $\mathbf{a}'$ . Optimal solutions then have the form  $(0, \mathbf{a}'_*)$  and  $(1, \bar{\mathbf{a}}'_*)$ . With this simplification, the PG of  $h_{3,3}^6(0, \mathbf{a}')$  has 14 vertices and 52 edges. Fig. 11 shows its embedding into the chip hardware.

#### IV. COMPLETE SET OF RAMSEY NUMBER RESULTS

Ref. 1 made three predictions that allow theory and experiment to be compared. The first is that the Ramsey number  $R(m, n)$  is the value of  $N$  at which the global minimum  $h_{min}$  of the cost function  $h_{m,n}^N(\mathbf{a})$  first becomes non-zero. The other two are, respectively, the value of the final ground-state energy  $E_{gs} = h_{min} \equiv \min_{\mathbf{a}} h_{m,n}^N(\mathbf{a})$  and its degeneracy  $D$ . For reference, Table I from the manuscript is included below which summarizes all our experimental results and the corresponding theoretical predictions. Examination of the Table shows that there is excellent agreement between the two.

In Secs. IV A and IV B we present our results for  $R(3, 3)$  and  $R(m, 2)$ . For each Ramsey number experiment, histograms of the final energies are presented. These energies are determined as follows. At the end of each quantum annealing run, the qubits are measured in the computational basis, and the outcome is the final spin variable-assignment  $\mathbf{s}$ . As explained in Sec. 4 of the manuscript, for those spin configurations satisfying the equality constraints, the spin configuration  $\mathbf{s}$  is translated back to the original binary  $\mathbf{a}$  variables. The energy  $E(\mathbf{a})$  is then calculated from the Ramsey energy function  $h_{m,n}^N(\mathbf{a})$  given in Sec. 3 of the manuscript, and its value entered into the appropriate histogram bin. For each Ramsey number experiment, energy histograms are presented over a range of  $N$  values. As in Sec. 4 of the manuscript, for each  $N$ , two histograms are given. The main histogram shows the energy function in terms of spins variable  $\mathbf{s}$ , where the energy function includes the Ramsey energy and the ferromagnetic interactions enforcing equality constraints between spins representing the same problem variable. The value of the ferromagnetic coupling strength  $\lambda$  used in the quantum annealing runs appears in the upper left corner of this histogram. The inset histogram corresponds to the  $\mathbf{a}$ -configurations, and displays the binned Ramsey energies  $E(\mathbf{a}) = h_{m,n}^N(\mathbf{a})$ . It is obtained from the spin configurations (of the main histogram) by filtering out those spin configurations not satisfying the equality constraints as these are infeasible (in the optimization sense) spin configurations. Each inset histogram contains the following information: (i) the set of observed Ramsey energies  $E$ , (ii) the probability (relative frequency) for the energy  $E$ , and (iii) the number of optimal  $\mathbf{a}$ -configurations that yielded the minimum energy  $E = h_{min}$ .

Having made these preliminary remarks we examine the remaining Ramsey number results.

### A. $\mathbf{R(3,3) = 6}$

As in the manuscript, two histograms are given for each  $N$ : the main histogram corresponds to spin energies that include contributions from the Ramsey energy function and the energy penalty functions that enforce the embedding of the primal graph vertices into the chip. As described above, the energy in the inset histograms is the Ramsey energy  $h_{m,n}^N(\mathbf{a})$ . The energy histograms for  $R(3,3)$  appear in Fig. 3.

Examining the inset histogram for  $N = 4$  we see that: (i)  $h_{min} = 0$ ; and (ii) 18 distinct  $\mathbf{a}$ -configurations have zero-energy, corresponding to 18 distinct graphs with no 3-cliques or 3-independent sets. From the main histogram we see that the probability to find an optimal  $\mathbf{a}$ -configuration is approximately 0.93. Note that  $h_{min} = 0$  is exactly the  $N = 4$  final ground-state energy  $E_{gs}(t_f) = 0$  found in Ref. 1, indicating that quantum annealing (QA) finds the final ground-state with high probability. The number of optimal graphs found agrees with that found numerically in Ref. 1.

A similar examination of the main histogram for  $N = 5$  gives: (i)  $h_{min} = 0$ ; and (ii) there are 12 optimal graphs/ $\mathbf{a}$ -configurations. From the main histogram we see that the probability to find an optimal  $\mathbf{a}$ -configuration is approximately 0.94. Again,  $h_{min} = 0$  equals the  $N = 5$  ground-state energy  $E_{gs}(t_f) = 0$  found in Ref. 1, and so QA finds the final ground-state with high probability. The number of optimal graphs found experimentally agrees with that found numerically in Ref. 1.

For  $N = 6$ , we see that: (i)  $h_{min} = 2$ ; and (ii) 1758 optimal graphs were observed. From the main histogram we see that the probability to find an optimal  $\mathbf{a}$ -configuration is approximately 0.91. As shown in Ref. 1,  $E_{gs}(t_f) = 2$  for  $N = 6$ , and so  $h_{min} = E_{gs}(t_f)$ , and QA again finds the final ground-state with high probability. Since  $N = 6$  is the first  $N$  value for which  $h_{min} = E_{gs}(t_f) > 0$ , the protocol for the Ramsey quantum algorithm correctly[6] identifies  $R(3,3) = 6$ . Finally, Ref. 1 showed that the number of optimal graphs for  $N = 6$  is 1760 so that QA found all but two of the 1760 optimal graphs.

Table I summarizes all of the above results.

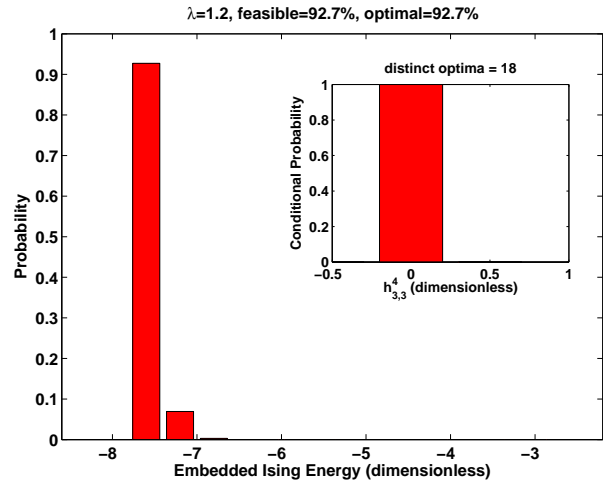
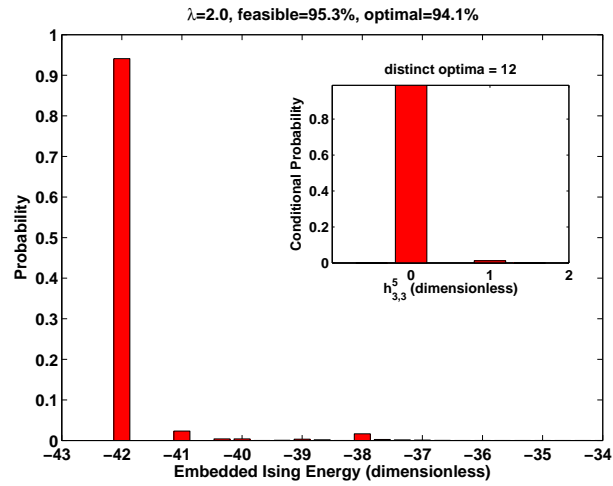
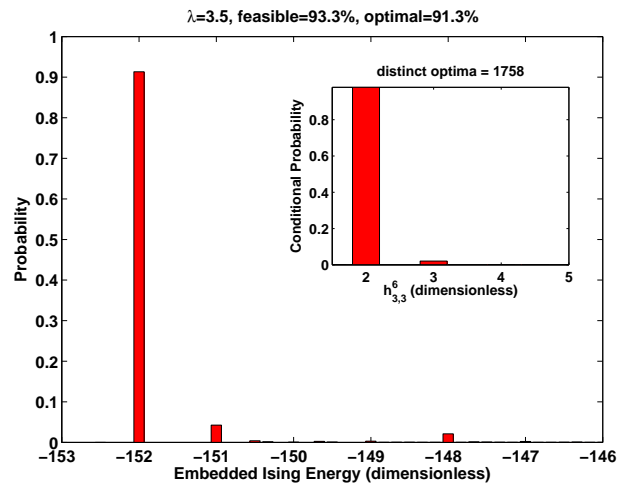
### B. $\mathbf{R(m,2) = m}$

Here we present our experimental results for  $R(m,2)$  with  $4 \leq m \leq 8$ . Since the  $R(m,2)$  discussion closely parallels that of  $R(3,3)$ , we give a more abbreviated presentation. In Section III above we showed that for  $N < m$ , the cost function  $h_{m,2}^N(\mathbf{a})$  is linear in  $\mathbf{a}$  and consequently the spins are uncoupled when this cost function is translated to spin variables  $\mathbf{s}_a$ . There is thus no need to introduce ancillary  $\mathbf{s}_b$ -spins, nor do we need to include ferromagnetic equality penalties in the Ising model. For this reason all spin configurations are feasible for  $N < m$ , and no  $\lambda$  values are recorded in the main histograms. All results below are included in Table I.

**R(4,2)** : Fig. 4 contains the energy histograms for  $R(4,2)$ . Examining the inset histogram for  $N = 3$  (4), we see that: (i)  $h_{min} = 0$  (1); (ii) the number of optimal graphs is 1 (7); and (iii) from the main histogram, the probability to find an optimal  $\mathbf{a}$ -configuration is approximately 1.0 (0.97). The minimum energies  $h_{min} = 0$  and 1 for  $N = 3$  and 4 agree exactly with the corresponding final ground-state energies  $E_{gs}(t_f)$  found in Ref. 1, indicating that QA finds the final ground-state with high probability. As  $h_{min}$  jumps from  $0 \rightarrow 1$  as  $N$  goes from  $3 \rightarrow 4$ , the Ramsey protocol correctly[6] identifies  $R(4,2) = 4$ . Finally, Ref. 1 showed that the number of optimal graphs for  $N = 3$  and 4 are, respectively, 1 and 7, which agrees with the number of optimals found by QA. For  $N = 3$ , the unique optimal graph is the fully connected 3-vertex graph which has no 4-cliques or 2-independent sets, while for  $N = 4$ , the optimal graphs are the  $\binom{4}{2} = 6$  graphs with a single 2-independent set and no 4-clique, and the unique fully connected 4-vertex graph which has one 4-clique and no 2-independent set.

**R(5,2)** : Fig. 5 contains the energy histograms for  $R(5,2)$ . Examining the inset histogram for  $N = 4$  (5), we see that: (i)  $h_{min} = 0$  (1); (ii) the number of optimal graphs is 1 (11); and (iii) from the main histogram, the probability to find an optimal  $\mathbf{a}$ -configuration is approximately 1.0 (0.76). The minimum energies  $h_{min} = 0$  and 1 for  $N = 4$  and 5 agree exactly with the corresponding final ground-state energies  $E_{gs}(t_f)$  found in Ref. 1, indicating that QA finds the final ground-state with high probability. As  $h_{min}$  jumps from  $0 \rightarrow 1$  as  $N$  goes from  $4 \rightarrow 5$ , the Ramsey protocol correctly[6] identifies  $R(5,2) = 5$ . Finally, Ref. 1 showed that the number of optimal graphs for  $N = 4$  and 5 are, respectively, 1 and 11, which agrees with the number of optimals found by QA. For  $N = 4$ , the unique optimal graph is the fully connected 4-vertex graph which has no 5-cliques or 2-independent sets, while for  $N = 5$ , the optimal graphs are the  $\binom{5}{2} = 10$  graphs with a single 2-independent set and no 5-clique, and the unique fully connected 5-vertex graph which has one 5-clique and no 2-independent set.

**R(6,2)** : Fig. 6 contains the energy histograms for  $R(6,2)$ . Examining the inset histogram for  $N = 5$  (6), we see

(a)  $N = 4$ (b)  $N = 5$ (c)  $N = 6$ FIG. 3: Energy histograms for  $R(3, 3)$  with  $N = 4, 5, 6$ .

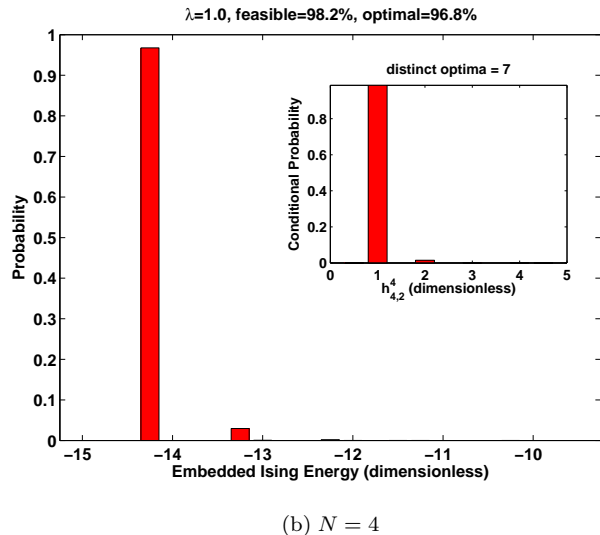
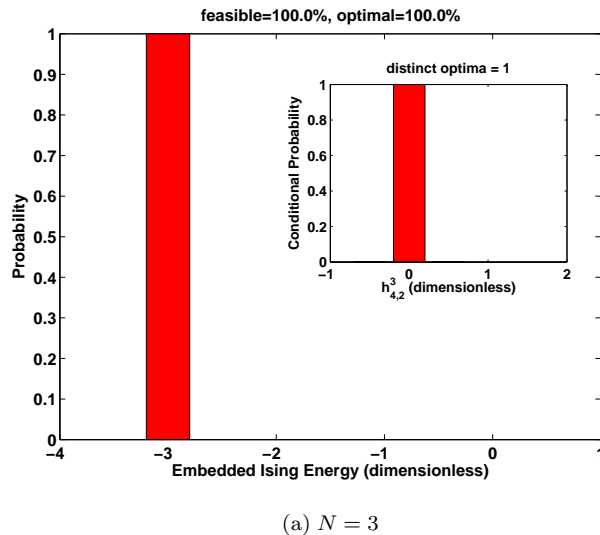


FIG. 4: Energy histograms for  $R(4, 2)$  with  $N = 3$  and 4.

that: (i)  $h_{min} = 0$  (1); (ii) the number of optimal graphs is 1 (16); and (iii) from the main histogram, the probability to find an optimal  $\mathbf{a}$ -configuration is approximately 1.0 (0.82). The minimum energies  $h_{min} = 0$  and 1 for  $N = 5$  and 6 agree exactly with the corresponding final ground-state energies  $E_{gs}(t_f)$  found in Ref. 1, indicating that QA finds the final ground-state with high probability. As  $h_{min}$  jumps from  $0 \rightarrow 1$  as  $N$  goes from  $5 \rightarrow 6$ , the Ramsey protocol correctly[6] identifies  $R(6, 2) = 6$ . Finally, Ref. 1 showed that the number of optimal graphs for  $N = 5$  and 6 are, respectively, 1 and 16, which agrees with the number of optimals found by QA. For  $N = 5$ , the unique optimal graph is the fully connected 5-vertex graph which has no 6-cliques or 2-independent sets, while for  $N = 6$ , the optimal graphs are the  $\binom{6}{2} = 15$  graphs with a single 2-independent set and no 6-clique, and the unique fully connected 6-vertex graph which has one 6-clique and no 2-independent set.

**R(7, 2)** : Fig. 7 contains the energy histograms for  $R(7, 2)$ . Examining the inset histogram for  $N = 6$  (7), we see that: (i)  $h_{min} = 0$  (1); (ii) the number of optimal graphs is 1 (22); and (iii) from the main histogram, the probability to find an optimal  $\mathbf{a}$ -configuration is approximately 1.0 (0.66). The minimum energies  $h_{min} = 0$  and 1 for  $N = 6$  and 7 agree with the corresponding final ground-state energies  $E_{gs}(t_f)$  found in Ref. 1, indicating that QA finds the final ground-state with high probability. As  $h_{min}$  jumps from  $0 \rightarrow 1$  as  $N$  goes from  $6 \rightarrow 7$ , the Ramsey protocol correctly[6] identifies  $R(7, 2) = 7$ . Finally, Ref. 1 showed that the number of optimal graphs for  $N = 6$  and 7 are,



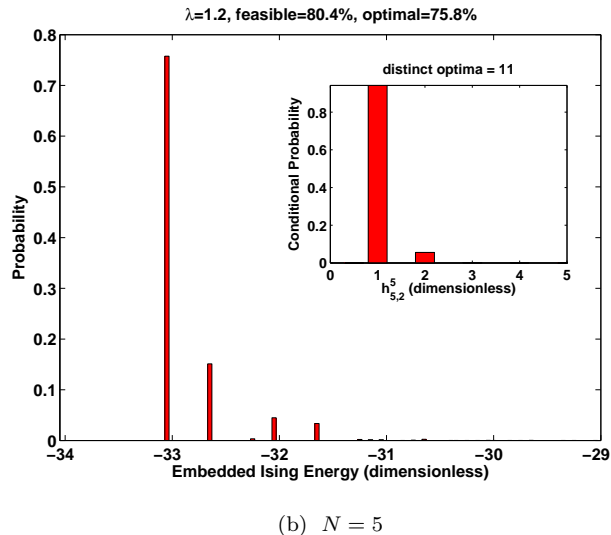
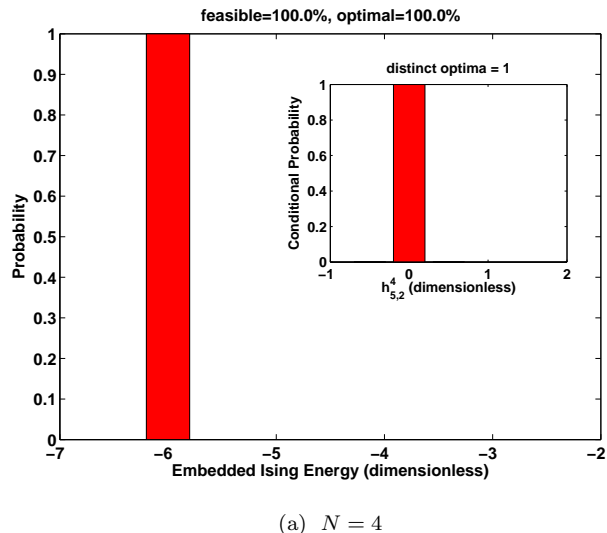
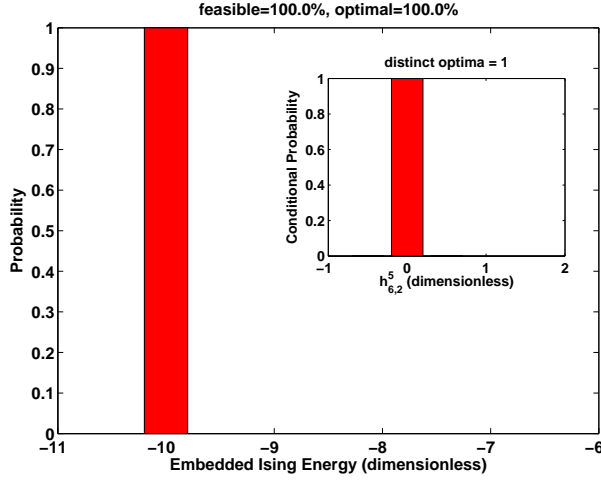


FIG. 5: Energy histograms for  $R(5, 2)$  with  $N = 4$  and 5.

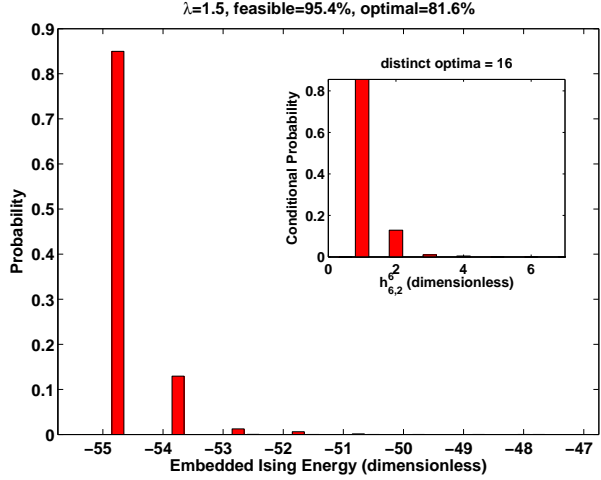
respectively, 1 and 22, which agrees with the number of optimals found by QA. For  $N = 6$ , the unique optimal graph is the fully connected 6-vertex graph which has no 7-cliques or 2-independent sets, while for  $N = 7$ , the optimal graphs are the  $\binom{7}{2} = 21$  graphs with a single 2-independent set and no 7-clique, and the unique fully connected 7-vertex graph which has one 7-clique and no 2-independent set.

**R(8, 2)** : Fig. 8 contains the energy histograms for  $R(8, 2)$ . Examining the inset histogram for  $N = 6$  we see that: (i)  $h_{min} = 0$ ; and (ii) a single  $\mathbf{a}$ -configuration has zero-energy, corresponding to the fully connected 6-vertex graph which has no 8-clique or 2-independent sets. From the main histogram we see that the probability to find an optimal  $\mathbf{a}$ -configuration is 1.0. Note that  $h_{min} = 0$  is exactly the  $N = 6$  final ground-state energy  $E_{gs}(t_f) = 0$  found in Ref. 1, indicating that quantum annealing (QA) finds the final ground-state with high probability. The number of optimal graphs found experimentally agrees with that found in Ref. 1.

A similar examination of the main histogram for  $N = 7$  gives: (i)  $h_{min} = 0$ ; and (ii) a single optimal graph/ $\mathbf{a}$ -configuration. The unique optimal graph is the fully connected 7-vertex graph which has no 8-clique or 2-independent set. From the main histogram we see that the probability to find an optimal  $\mathbf{a}$ -configuration is 1.0. Again,  $h_{min} = 0$  equals the  $N = 7$  ground-state energy  $E_{gs}(t_f) = 0$  found in Ref. 1, and so QA finds the final ground-state with high probability. The number of optimal graphs found experimentally agrees exactly with that found in Ref. 1.



(a)  $N = 5$



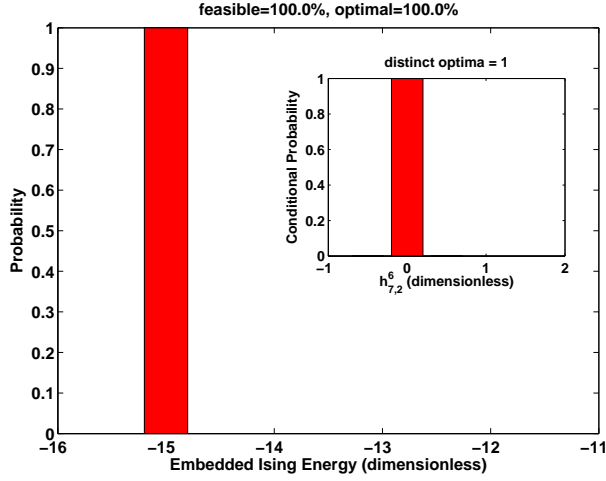
(b)  $N = 6$

FIG. 6: Energy histograms for  $R(6, 2)$  with  $N = 5$  and 6.

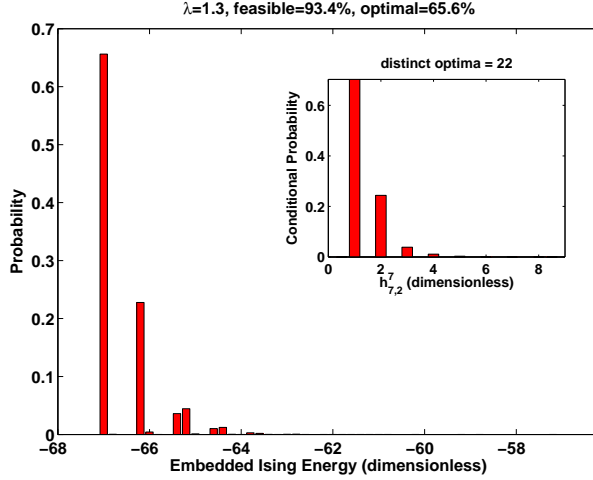
For  $N = 8$ , we see that: (i)  $h_{min} = 1$ ; and (ii) 29 optimal graphs were observed. Here the optimal graphs are the  $\binom{8}{2} = 28$  graphs with a single 2-independent set and no 8-clique, and the unique fully connected 8-vertex graph which has one 8-clique and no 2-independent set. From the main histogram we see that the probability to find an optimal  $\mathbf{a}$ -configuration is approximately 0.65. As shown in Ref. 1,  $E_{gs}(t_f) = 1$  for  $N = 8$ , and so  $h_{min} = E_{gs}(t_f)$ , and QA again finds the final ground-state with high probability. Since  $N = 8$  is the first  $N$  value for which  $h_{min} = E_{gs}(t_f) > 0$ , the protocol for the Ramsey quantum algorithm correctly[6] identifies  $R(8, 2) = 8$ . Finally, Ref. 1 showed that the number of optimal graphs for  $N = 8$  is 29 so that QA found all of the optimal graphs.

### V. EMBEDDING PRIMAL GRAPH INTO CHIP HARDWARE

Fig. 2 reproduces Fig. 1 of the manuscript which is included here for convenience. As discussed in Section II, the primal graph of an optimization cost function consists of: (i) vertices that represent bit variables whose values are to be optimized; and (ii) edges that connect pairs of interacting bits. The primal graph of  $h_{m,n}^N(\mathbf{s})$  is the same as the primal graph of  $h_{m,n}^N(\mathbf{a})$  as the former is obtained from the latter by the substitution  $\mathbf{s} = 2\mathbf{a} - 1$ .



(a)  $N = 6$



(b)  $N = 7$

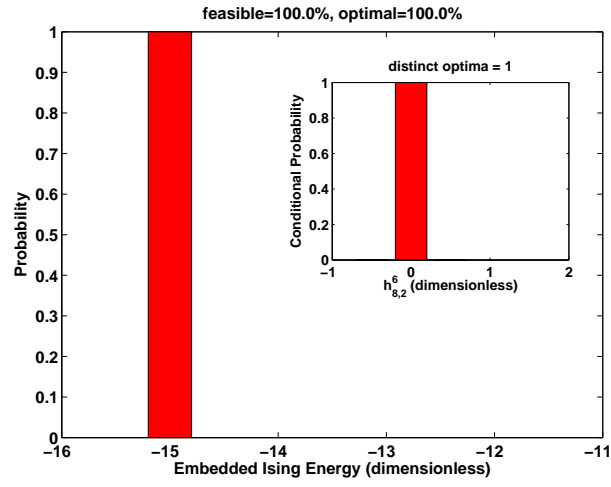
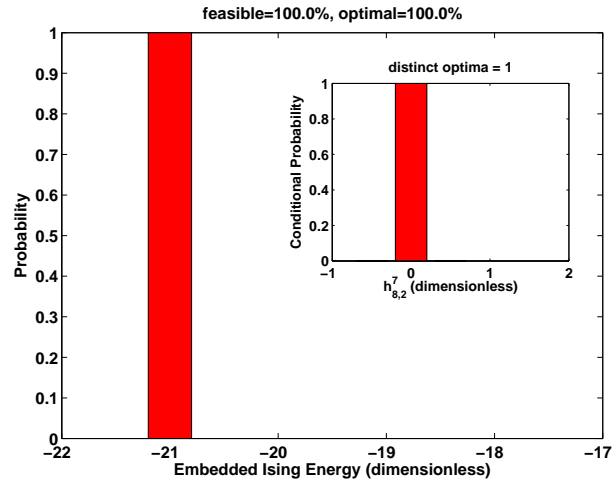
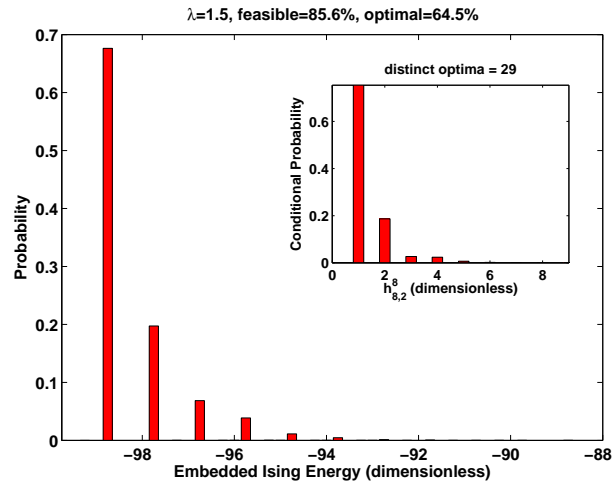
FIG. 7: Energy histograms for  $R(7, 2)$  with  $N = 6$  and 7.

### A. $R(8, 2)$

The Ramsey cost function  $h_{8,2}^8(\mathbf{a})$  is quite complicated as it involves a term that couples 28 spin variables. As discussed in Section III above this requires the introduction of 26 ancillary  $\mathbf{b}$ -variables to reduce this product to a sum of pairwise interactions. The resulting primal graph for  $h_{8,2}^8(\mathbf{a}, \mathbf{b})$  is shown in Fig. 9. For this case there are a total of 54 primal  $\mathbf{a}$  and  $\mathbf{b}$  variables. The embedding of the primal graph in Fig. 9 into the chip is shown in Fig. 10. Note that an additional 30 qubits are needed to complete the embedding, bringing the total number of qubits used in the computation to 84. Like-colored qubits represent a single primal variable, though note that certain colors had to be reused. As before black edges carry the primal variable couplings. The topmost qubit labeled 5 in Fig. 10 corresponds to qubit 17 of Fig. 2.

### B. $R(m, 2)$ for $4 \leq m \leq 7$

The procedure for finding the chip embeddings for the Ramsey cost functions  $h_{m,2}^m$  with  $m = 4, \dots, 7$  is similar to that presented for  $h_{8,2}^8$ . The resulting embeddings are much simpler and are not reproduced here.

(a)  $N = 6$ (b)  $N = 7$ (c)  $N = 8$ FIG. 8: Energy histograms for  $R(8, 2)$  with  $N = 6, 7, 8$ .

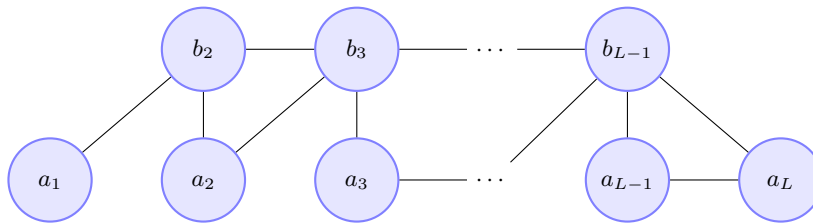


FIG. 9: Primal graph for  $h_{m,2}^m(\mathbf{a}, \mathbf{b})$ .  $L = \binom{m}{2}$  is the total number of  $\mathbf{a}$  variables.

### C. $R(3,3)$

As explained in Section 3 above, the cost function  $h_{3,3}^6(\mathbf{a})$  has 14 variables since we fixed  $a_1 = 0$ . Fig. 11 shows the embedding of the primal graph for the problem  $h_{3,3}^6(0, a_2, a_3, \dots, a_{15})$ . Note that the qubit labeled  $i$  in this Figure corresponds to the binary variable  $a_{i+1}$ . Like-colored qubits are connected with ferromagnetic couplings of strength  $\lambda$  along the like-colored edges. Black edges are used to represent the coupling strengths between primal variables. The embedding is situated within the chip so that the top-left qubit labeled as 8 in Fig. 11 corresponds to qubit 41 of Fig. 2. Note that many other embeddings into the chip are possible, and we make no claims that this embedding uses the smallest numbers of qubits to represent the required connectivity.

## VI. DISCUSSION

In this Section we discuss a number of important topics related to the Ramsey number experiments and their analysis.

### A. Parameter noise

Parameter noise enters during the programming of the quantum annealing (QA) Hamiltonian  $H(t)$  onto the chip and this noise is frozen into the actual value the local fields  $\mathbf{h}$  and coupling constants  $\mathbf{J}$  take on. By this we mean that the actual value of (say) the local field  $\mathbf{h}_a = \mathbf{h}_0 + \Delta\mathbf{h}$ , where  $\mathbf{h}_0$  is the nominal value we would like  $\mathbf{h}$  to take plus an error  $\Delta\mathbf{h}$ . It is important to understand that, because the chip is programmed only once,  $\Delta\mathbf{h}$  does not change from one QA run to the next. Thus the effect of parameter noise is to produce a small static random shift in  $\mathbf{h}$  and  $\mathbf{J}$  away from nominal values  $\mathbf{h}_0$  and  $\mathbf{J}_0$ , but which remains fixed from one QA run to the next. Now if the lowest-lying instantaneous energies  $E(t)$  associated with the QA Hamiltonian  $H(t)$  vary rapidly with small changes in  $\mathbf{h}$  and  $\mathbf{J}$ , then hardware performance on the optimization problem associated with  $H(t)$  can be expected to be sensitive to parameter noise. The indication of this would be disagreement between the theoretical predictions based on  $\mathbf{h} = \mathbf{h}_0$  and  $\mathbf{J} = \mathbf{J}_0$ , and the experimental results based on the shifted values  $\mathbf{h}_a$  and  $\mathbf{J}_a$ . On the other hand, if the low-lying energy landscape does not vary rapidly with small changes in  $\mathbf{h}$  and  $\mathbf{J}$ , then hardware performance should be well-described by the nominal parameters  $\mathbf{h}_0$  and  $\mathbf{J}_0$  and so theoretical predictions and experimental results should have strong agreement, and hardware performance should not be sensitive to parameter noise.

Note that in the Ramsey number experiments reported in the manuscript and in this SI: (i) all Ramsey numbers  $R(m, 2)$  with  $4 \leq m \leq 8$  and  $R(3, 3)$  were found correctly; (ii) all final ground-state energies  $E_{gs}(T)$  were found correctly; and (iii) for  $R(m, 2)$ , and for  $R(3, 3)$  with  $N = 4$  and 5, all Ramsey ground-states were found correctly, and for  $R(3, 3)$  with  $N = 6$ , 1758 out of 1760 ground-states were found correctly. It is possible to conclude this as exact theoretical results were available to check against experimental results [1]. As noted above, the excellent agreement between theory and experiment is an indication that the Ramsey number experiments are not very sensitive to parameter noise. Another way to understand this lack of sensitivity is to note that the Ramsey energy functions appearing in Section III above all involve  $\mathbf{h}$  and  $\mathbf{J}$  values that are small integers, and these small integer values are safely within the hardware's available parameter precision.



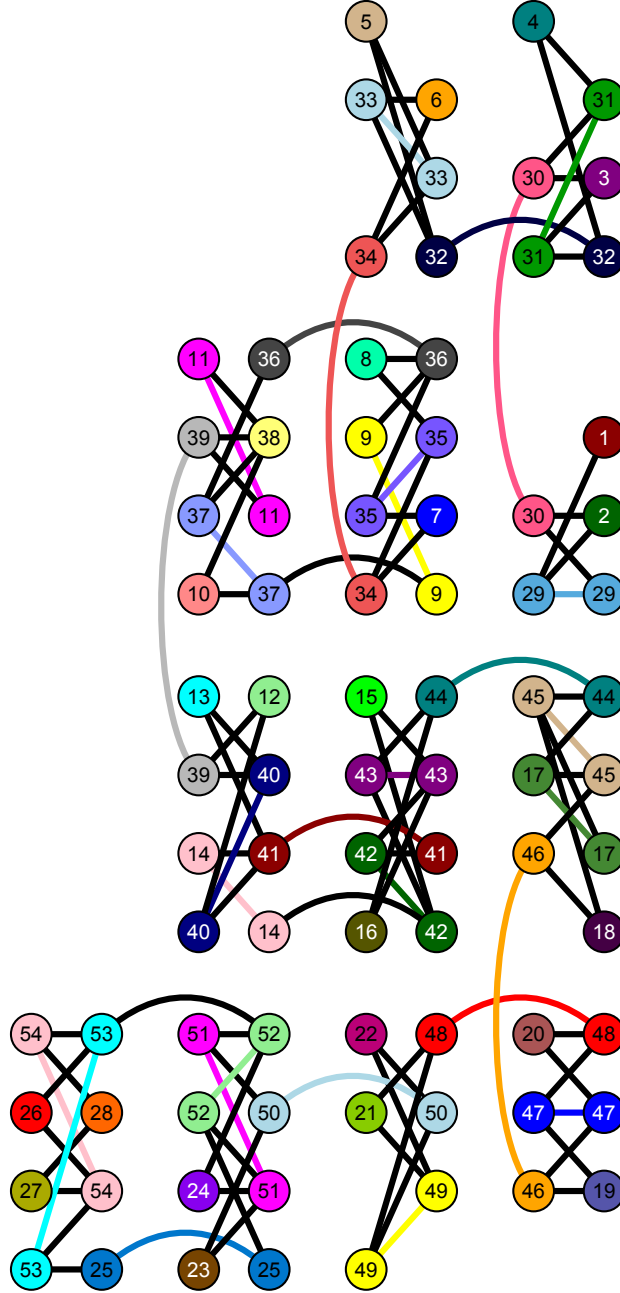


FIG. 10: **Embedding of the primal graph of Fig. 9 into hardware.** Qubits are numbered so that qubits labeled  $i$  with  $1 \leq i \leq 28$  correspond to primal variables  $a_i$ , and qubits labeled  $29, \dots, 54$  correspond to the ancillary variables  $b_2, \dots, b_{27}$ .

### B. Distribution of final energies

Recall from Table I above that the final Ramsey ground-state (GS) is highly degenerate so that the final gap vanishes:  $\Delta(t_f) = 0$ . Thus as  $t \rightarrow t_f$ , the lowest energy-levels get arbitrarily close to each other and so transitions out of the GS become more and more likely. However, as  $t \rightarrow t_f$ , there remains little time for the hardware to relax back to the final GS before the quantum annealing (QA) run completes. Thus one can anticipate that the final distribution of energies will not correspond to a thermal equilibrium distribution described by an effective temperature  $T_e$ . This is

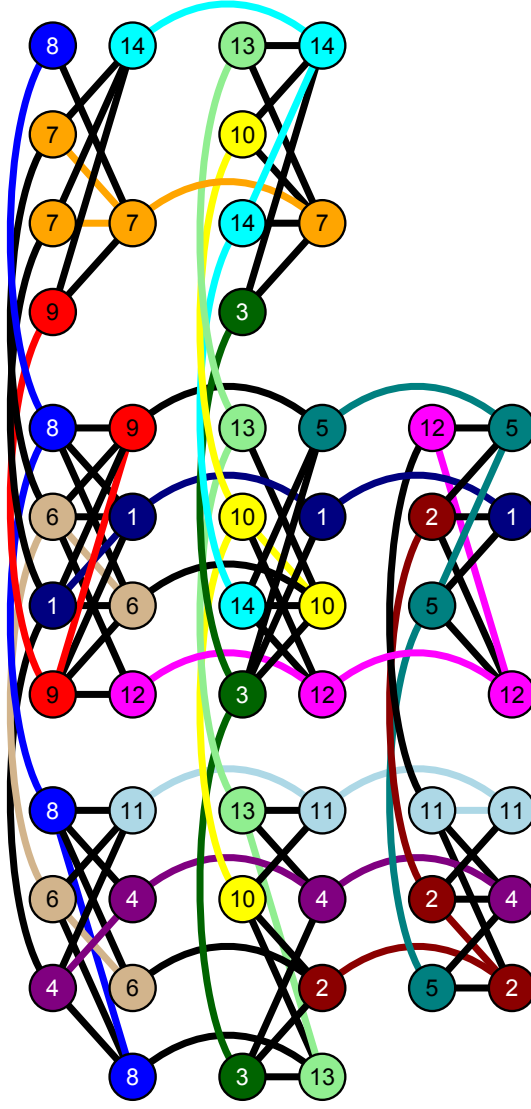


FIG. 11: **Embedding of the primal graph of  $h_{3,3}^6(0, a_2, a_3, \dots, a_{15})$  into hardware.** Variable  $a_{i+1}$  is labeled as qubit  $i$ .

in fact the case as can be seen in Fig. 12 which is a parametric plot of Boltzmann versus empirical probabilities for the  $R(8, 2)$  data with  $N = 8$ . Here each data point corresponds to a particular spin/ancilla configuration  $(\mathbf{a}, \mathbf{b})$  whose: (i) x-coordinate is its empirical probability  $P_e$  which is the fraction of QA runs in which  $(\mathbf{a}, \mathbf{b})$  was the outcome of the final measurement; and (ii) y-coordinate is the Boltzmann probability  $P_B(\mathbf{a}, \mathbf{b}) = \exp[-E(\mathbf{a}, \mathbf{b})/T_e]/Z$ . In the Boltzmann distribution,  $E(\mathbf{a}, \mathbf{b})$  is the hardware embedded Ramsey energy including ancilla contributions;  $T_e$  is an effective temperature found by doing a maximum likelihood Boltzmann fit to the empirical data; and  $Z$  is the partition function. The fit yielded  $T_e = 0.2831$  in the dimensionless units of the problem Hamiltonian whose energy scale is set by the maximum value of the coupling constants  $\mathbf{J}$  which is 1. Notice that the data points line up along a number of horizontal lines, with each line having the same Boltzmann probability  $P_B(E)$ . Each horizontal line thus corresponds to spin/ancilla configurations with the same Ramsey energy  $E$ . If the final distribution of energies corresponded to thermal equilibrium, spin configurations with the same energy  $E$  would have the same empirical probability  $P_e$ , and so each horizontal line would collapse to a single point on the  $P_B(E) = P_e(E)$  line. Said another way, we see that spin/ancilla configurations with the same energy have different empirical probabilities which indicates unequivocally that the final distribution of energies does not correspond to thermal equilibrium. As explained above, this is not unexpected given that the gap  $\Delta(t \rightarrow t_f) \rightarrow 0$  so that transitions out of the GS become highly likely as  $t \rightarrow t_f$ , and little time is left for the hardware to relax back to the GS.

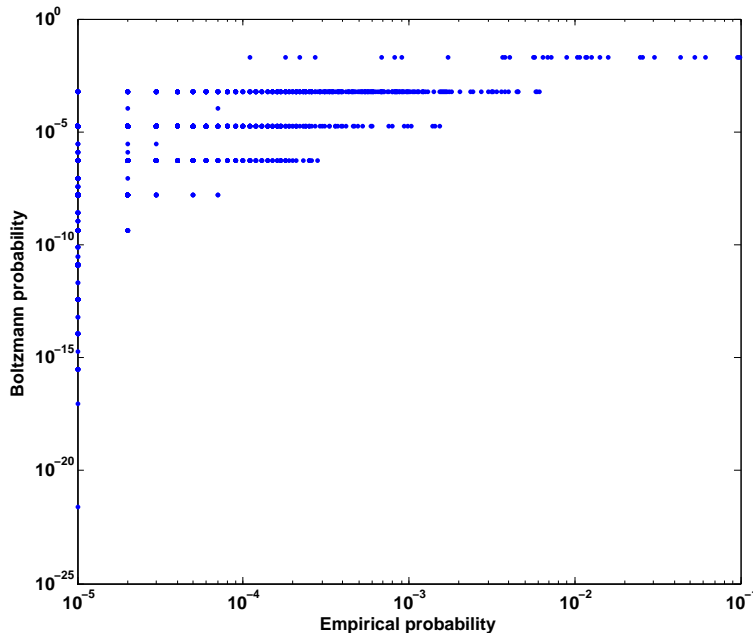


FIG. 12: Plot of Boltzmann probability versus empirical probability for  $R(8, 2)$  with  $N = 8$ . See text for full discussion.

### C. Quantum annealing rate

For a given Ramsey number experiment, the initial and problem Hamiltonians are programmed onto the chip and remain fixed throughout all 100,000 quantum annealing (QA) runs. As noted in Section 2 of the manuscript, the time rate of change of the instantaneous Hamiltonian  $H(t)$  is controlled through the annealing profiles  $A(t)$  and  $B(t)$  that drive the QA run. Slowing the variation of  $A(t)$  and  $B(t)$  would make the QA run more adiabatic, and thus would reduce the probability of finding the hardware in an excited state in the final measurement, and the distribution of final energies closer to a thermal equilibrium distribution. The rates chosen for the experiments reported in the manuscript and in the SI balance the need to execute a QA run in a reasonable amount of time, and the need to have a significant fraction of the QA runs find the hardware in the final ground-state (GS). Inspection of the histograms in the manuscript and the SI shows that the probability  $P_{success}$  of finding the hardware in the final GS satisfies  $0.645 \leq P_{success} \leq 1.000$ . These probabilities are quite high and indicate that the choices made for  $A(t)$  and  $B(t)$  are a reasonable compromise between competing interests. Further reduction of these rates would act to increase the lower bound on  $P_{success}$ , which is already quite high. Note that the Ramsey experiments were carried out with an annealing time of  $1000\mu s$ . The D-Wave hardware allows annealing times as short as  $5\mu s$ , and annealing at these faster rates is found to reduce the success probability  $P_{success}$  as expected.

### D. Choosing the spin-chain ferromagnetic coupling

For a particular Ramsey number, the experimental procedure begins by setting the ferromagnetic (FM) coupling parameter  $\lambda$  to a small initial value. Then 100,000 QA runs are done with this  $\lambda$  value and the qubits measured at the end of each run. The fraction of these runs  $F$  in which the equality constraints are satisfied is then determined. If  $F$  is less than 0.85, the value of  $\lambda$  is increased and another 100,000 QA runs are carried out and the qubits measured. This process continues until  $F$  is first found to be greater than 0.85. At this point  $\lambda$  is increased one last time and it is this value of  $\lambda$  that is used in the experiments and listed at the top of each histogram. As noted above, the (at most) 15% of QA runs which did not satisfy the equality constraints are discarded as, for these runs, the FM chains do not act as a single “logical” qubit and so do not properly capture the physics that couples distant qubits in the manner required by the Ramsey problem Hamiltonian. Only the (at least) 85% of runs which did satisfy the equality constraints properly represent the Ramsey Hamiltonian and so only those runs are kept as data and analyzed. That is why these runs were referred to as feasible spin-configurations in the manuscript and SI. Of these feasible spin

configurations, some fraction has the lowest measured energy and these are the candidate ground-states (GS). The fraction of the 100,000 QA runs that is feasible and lowest energy (viz. optimal) is the probability listed as “optimal = 0.xxx” in Figures 2 and 3 of the paper, and Figures 3-8 of the SI. We will describe the calculation of this optimal probability in detail in Section [VIE](#). For the Ramsey numbers considered in the manuscript, we know the final GS energy in all cases from either numerical simulations or analytical calculations (see Ref. 3 of the manuscript). Thus we can conclude that the experiments found the GS energy correctly and with high probability. In summary, the (at most) 15% of QA runs that violated the equality constraints never influence the data that is analyzed to determine the experimental results reported in the manuscript and the SI and so cannot cause an error in any of these results.

### E. Probability for optimal spin-configuration

All histograms appearing in the manuscript and SI report the probability that a Ramsey experiment yields an optimal Ising spin configuration: “optimal = 0.xxx”. For example, in Figure 2(b) of the manuscript, the 64.5% is found as follows. We see at the top of that figure that of the 100,000 QA runs, 85.6% were feasible (as defined in Sec. [VID](#)) spin-configurations. From the inset histogram we can read off that approximately 75% of the feasible spin-configurations were also optimal (viz. had the smallest energy). Thus the fraction of total runs that were feasible and optimal is approximately  $0.856 \times 0.75 = 0.642$ . The actual value is 0.645 which is the 64.5% quoted as optimal at the top of Figure 2(b). This same analysis is done for each Ramsey number to calculate the percentage of QA runs that yield optimal and feasible spin-configurations, and that percentage appears at the top of the corresponding histogram.

### F. Classical annealing

Here we show that classical/thermal annealing can be ruled out as the source of optimization efficacy. First, it is clear that the hardware is not realizing classical annealing since the final distribution of low energy states is not Boltzmann distributed as discussed in Sec. [VIB](#) above, and furthermore, the temperature of the hardware is never varied during the experiments. Finally, we compare the optimization efficacy of the quantum annealing hardware with that of an efficient C-implementation of simulated annealing that was run on a standard 8Gb, 2.66GHz desktop computer. The results of Fig. [13](#) show that at a runtime of 2.5ms (which is the 1ms runtime plus 1.5ms read-out time of the Ramsey number experiments), the quantum annealing hardware obtains significantly higher success rates for finding both feasible and optimal final spin-configurations than does simulated annealing.

### G. Hardware quantum coherence

Since an adiabatic quantum optimization (AQO) algorithm encodes the problem solution in the ground-state (GS) of the problem Hamiltonian, this class of quantum algorithms does not make use of a coherent superposition of instantaneous energy-levels. Said another way, the relative phases of the different instantaneous energy-levels in such a superposition contain no useful information about the optimization problem solution. Instead, the ability of the adiabatic quantum dynamics to drive the system state to the GS of the problem Hamiltonian directly impacts the performance of the AQO algorithm. Thus a more useful performance metric for an AQO algorithm is the Uhlmann fidelity  $F = (1/\sqrt{P_0})\text{Tr}\sqrt{\sqrt{\rho_0}\rho_s\sqrt{\rho_0}}$  which is the overlap of the reduced density matrix  $\rho_s$  with a target density matrix  $\rho_0$ . In the context of an AQO problem,  $P_0$  is the probability for the quantum annealing (QA) processor/chip to be in the GS of the problem Hamiltonian at time  $t = T$ ;  $\rho_0 = |E_g(T)\rangle\langle E_g(T)|$  is the density matrix associated with the target state  $|E_g(T)\rangle$  which is the GS of the problem Hamiltonian at  $t = T$ ; and  $\rho_s$  is the reduced density matrix of the QA processor at  $t = T$ . A study of the performance of adiabatic quantum computation using the Uhlmann fidelity as the performance metric has been carried out in Ref. [7](#). We refer the reader to this paper for a detailed examination of this question. Still, it is of interest to come to a better understanding of quantum coherence in the D-Wave hardware (viz. phase coherence and entanglement). A demonstration of such coherence requires a dedicated experimental effort which is currently underway at D-Wave, and the results of that work will be reported elsewhere. We stress that the focus of this paper has been: (i) a specific application of a QA processor; and (ii) the development of techniques which will allow in principle the solution of arbitrary discrete optimization problems by QA of sparsely-connected Ising models.

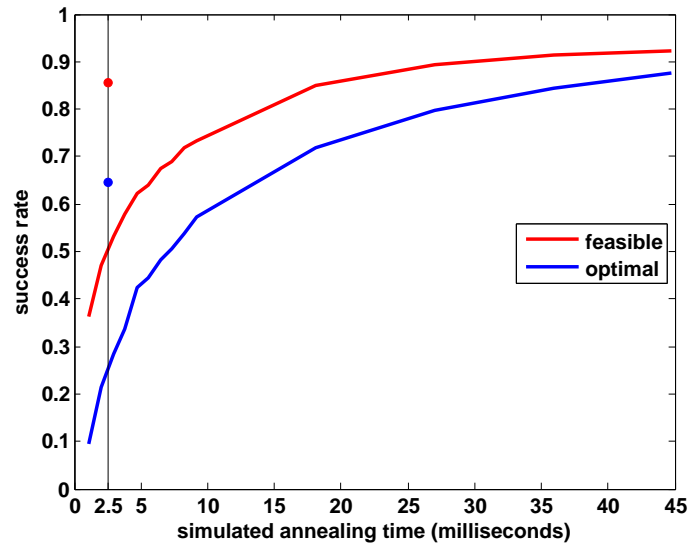


FIG. 13: Plot of simulated annealing (SA) success probability to determine optimal and feasible spin-configurations versus run-time for  $R(8, 2)$  at  $N = 8$ . The SA cooling schedule is exponential; and the initial and final temperatures were optimized for maximum success probability. For comparison, quantum annealing hardware results are also shown for a runtime of  $2.5\text{ms}$ . See text for further discussion.

- 
- [1] F. Gaitan, L. Clark. Ramsey numbers and adiabatic quantum computing. *Phys. Rev. Lett.* **108**, 010501 (2012).
  - [2] E. Farhi, J. Goldstone, S. Gutmann, M. Sipser. Quantum computation by adiabatic evolution. See <http://arxiv.org/abs/quant-ph/0001106>, 2000.
  - [3] J. Spencer, *Ten Lectures on the Probabilistic Method* (SIAM, ed. 2, Philadelphia, PA, 1994).
  - [4] Amin, M. H. S., Love, P. J., & Truncik, C. J. S., *Phys. Rev. Lett.* **100**, 060503 (2008).
  - [5] Amin, M. H. S., Truncik, C. J. S., & Averin, D. V., *Phys. Rev. A* **80**, 022303 (2009).
  - [6] B. Bolloás. *Modern Graph Theory* (Springer, New York, 1998).
  - [7] Q. Deng, D. V. Averin, M. H. Amin, and P. Smith, Decoherence induced deformation of the ground-state in adiabatic quantum computation, *Scientific Reports* **3**, Article number 1479 (2013); arXiv:1208.3515v1.